SUPERSONIC NOZZLE DESIGN FOR VISCOUS FLUIDS

Thesis by

George E. Gompf

In Partial Fulfillment of the Requirements

for the Degree of Aeronautical Engineer

California Institute of Technology

Pasadena, California

1949

ABSTRACT

A method is presented for including the effects of viscosity in the design of supersonic wind tunnel nozzles, the effect being presented in the form of a modification to the non-viscous, or perfect fluid, nozzle shapes. The modification essentially consists of providing additional expansion area to compensate for the retarded flow near the wall, and is estimated from considerations of possible boundary layer growth along a heat insulated flat wall with a pressure gradient, when both the velocity profile and friction coefficient are assumed.

It is shown that the modification to the perfect fluid shape becomes very pronounced for design Mach numbers above five and results in a shorter nozzle length for a given test section size than that predicted from perfect fluid theory. At a Mach number of 10, this method results in a nozzle length reduction of 50% indicating that the boundary layer occupies this percentage of the test section for the shortened nozzle.

Design curves are presented from which the modification to a specific perfect fluid nozzle shape may be computed for Mach numbers up to 10.

ACKNOWLEDGEMENTS

The author is greatly indebted to Dr. A. E. Puckett, who initiated this study and whose guidance and advice throughout the course of the investigation have been invaluable; to Dr. F. E. Marble, who suggested important refinements in the analysis; and to Miss Shirley Woodbury, who typed the manuscript.

TABLE OF CONTENTS

LIST OF FIGURES

PART I

INTRODUCTION AND ASSUMPTIONS

Supersonic nozzle design is concerned with the problem of producing uniform parallel flow of a compressible fluid at a desired velocity exceeding that of sound in the medium. To attain this velocity, the nozzle must consist of a contraction portion leading into the throat where sonic velocity is reached, followed by an expansion shape calculated to produce uniform flow at the nozzle exit. Several papers exist (References 1, 2, 3, 4) presenting graphical or exact analytical methods for the design of supersonic nozzles for perfect, or nonviscous fluids, but little information is available concerning the effects of viscosity upon the nozzle expansion shape.

This lack of information is understandable, for the addition of viscous and heat conduction terms to the equations of motion for a compressible fluid introduces such extreme mathematical complications that no general solutions have yet been obtained. Thus any attempt to consider viscous effects must utilize certain simplifying assumptions, which reduce the equations to forms which can be solved explicitly. Foremost among these simplifications is that due to Prandtl which leads to the concept of the boundary layer. Prandtl showed that, for fluids of low viscosity (i.e., flows at high Reynolds number), the effects of viscosity are essentially confined within a thin layer of the fluid adjacent to the solid boundaries of the flow field, while outside this thin "boundary layer" the fluid can be considered as non-viscous.

Applying the boundary layer theory to flow in a nozzle, the actual flow field can be regarded as consisting of a central core of non-viscous

or potential flow surrounded by a thin layer of retarded flow clinging to the nozzle walls. The "effective nozzle wall" for the potential flow field occurs inside the physical wall at a distance known as the displacement thickness of the boundary layer. Consequently, if the displacement thickness for a given flow can be computed and the physical wall displaced outward that much from the potential wall position, the resultant channel should produce the same flow exterior to the boundary layer as the original potential nozzle. Utilizing this result of the boundary layer assumption, the problem of supersonic nozzle design for viscous fluids is reduced to that of determining the rate of growth of the boundary layer displacement thickness along the potential nozzle length, together with the wall modification to the potential shape which will just compensate for this growth.

However, the boundary layer equations for a compressible fluid with a pressure gradient are still extremely difficult to solve, requiring further assumptions and simplifications to render a solution possible. Von Kármán (Ref. 5) introduced a simplification by showing that, if one is willing to abandon efforts to obtain the exact flow configuration within the boundary layer and instead satisfy the equations of motion only in the mean, the resultant equations are much simpler, but still give the boundary layer thickness to a very close approximation. This method determines the thickness by balancing the shear and pressure forces against the rate of momentum loss within a boundary layer having an assumed velocity profile. He has shown that the resultant thickness is relatively insensitive to moderate changes in the assumed velocity profile, consequently any plausible, simply defined profile may be utilized. Polhausen, in applying Kármán's momentum considerations to

the incompressible case, utilized for the profile form a polynomial in powers of distance along the solid boundary. However, this leads to extreme complications in the compressible case, making a simpler profile form highly desirable.

Puckett has shown that, with the assumption of an invariant profile shape, the boundary layer momentum relations can be reduced to a first order linear differential equation relating the boundary layer thickness with distance along the nozzle. The invariant velocity profile fixes the relation between the displacement thickness and the total thickness as a function of the free stream Mach number, which in turn determines the wall modification to the potential nozzle shape to compensate for the viscous effects.

Having chosen a velocity profile, the resulting boundary layer thickness becomes proportional to the wall friction coefficient, which must still be estimated from Reynolds number and Mach number considerations. However, by suitable choices of the velocity profile and friction coefficient, this method is equally valid for laminar or for turbulent boundary layers, a feature not possessed by the more rigorous analysis based on the Navier-Stokes equations.

The assumptions inherent in this specialized application of viscous fluid theory are rather numerous and should be clearly recognized. For that reason, they are enumerated below:

1. The air obeys the perfect gas laws, where the ratio of specific heats remains constant at $\gamma = 1.400$.
2. Flow is essentially one-dimensional, that is, wall curvature is very small and

$$\frac{v}{u} \ll 1 \quad , \quad \frac{\partial p}{\partial y} = \frac{\partial p}{\partial z} = 0$$

3. Viscous effects are confined within the boundary layer region having a sharply defined edge; outside this region, potential flow occurs.

4. The boundary layer velocity profile does not vary with position along the nozzle wall.

5. The nozzle wall is insulated and the Prandtl number has the value unity, thus the fluid at the wall recovers its stagnation temperature.

6. For a turbulent boundary layer, it is necessary to assume no heat transfer takes place in order to justify stagnation temperature recovery at the wall.

PART II

DETERMINATION OF BOUNDARY LAYER GROWTH

A. Derivation of the Boundary Layer Equations

Following von Kármán's method (Ref. 5), momentum considerations in the mean are applied to a fixed infinitesimal slice of the boundary layer on one parallel wall of an expanding two-dimensional channel. The boundary layer is thus subjected to a pressure gradient due to the velocity gradient in the outer or potential flow in the channel. An energy balance for the slice requires that the time rate of change of momentum in the x-direction within this wedge-shaped element must just balance the resultant component of the shear and pressure forces in the same direction on the faces of the element.

Referring to the notation given in the Appendix and to Fig. 1, showing the nozzle coordinate system for the boundary layer analysis, the forces acting on this element consist of:

a) the force on the left face $= ph\delta$

b) the force from the top face $= ph\frac{\partial \delta}{\partial x}dx$

c) the force from the side face $= p\delta\frac{\partial h}{\partial x}dx$

d) the force on the right face $= -ph\delta - \frac{\partial}{\partial x}(ph\delta)dx$

where only first order terms have been retained. The net pressure force to the right is the sum of these four terms or

$$ph\delta + ph\frac{\partial\delta}{\partial x}dx + p\delta\frac{\partial h}{\partial x}dx - ph\delta - \frac{\partial}{\partial x}(ph\delta)\,dx$$

$$= p\frac{\partial}{\partial x}(h\delta)\,dx - p\frac{\partial}{\partial x}(h\delta)\,dx - h\delta\frac{\partial p}{\partial x}dx$$

$$= -h\delta\frac{\partial p}{\partial x}dx \quad .$$

Note that the forces on the slanting faces cancel identically, leaving as the only pressure force the term arising from the pressure gradient acting on the rectilinear "core" of the boundary layer slice.

The surface friction or shear on the bottom face contributes a force in the x-direction of

$$-h\tau_o\,dx$$

while the top face, being adjacent to the potential flow, has no surface friction. The shear on the side of the slice can be neglected since it is an inherent assumption of the boundary layer concept that the thickness δ is small compared to the other physical dimensions.

Thus the net force to the right is

$$-h\tau_o\,dx - h\delta\frac{\partial p}{\partial x}dx \quad .$$

For steady flow, the momentum change within this fixed slice is the difference between that carried in through the top and left face, and that carried out through the right face. This momentum change can be more easily obtained if, in anticipation of the integrals involved, the momentum and displacement thicknesses are introduced at this point, as defined respectively by

$$\vartheta = \int_0^{\delta} \frac{\rho u}{\rho_1 u_1}\left(1 - \frac{u}{u_1}\right)dy \qquad (1)$$

$$\delta^* = \int_0^\delta \left(1 - \frac{\rho u}{\rho_1 u_1}\right) dy \qquad (2)$$

The displacement thickness of the boundary layer has the physical significance that the reduction in mass flow through the boundary layer is equivalent to an inward shift or displacement of the wall by that amount. Similarly, the momentum thickness might represent the wall shift proportional to the percentage momentum loss in the boundary layer. Equations (1) and (2) can be manipulated to resemble the integrals arising in the momentum derivation.

$$\rho_1 u_1 \delta^* = \int_0^\delta (\rho_1 u_1 - \rho u)\, dy = \rho_1 u_1 \delta - \int_0^\delta \rho u\, dy$$

or

$$\int_0^\delta \rho u\, dy = \rho_1 u_1 (\delta - \delta^*) \qquad (3)$$

$$\rho_1 u_1^2 \vartheta = \int_0^\delta \rho u (u_1 - u)\, dy = u_1 \int_0^\delta \rho u\, dy - \int_0^\delta \rho u^2\, dy$$

or that

$$\int_0^\delta \rho u^2\, dy = \rho_1 u_1^2 (\delta - \delta^* - \vartheta) \qquad (4)$$

Returning now to a consideration of the momentum change within the element, the momentum carried in through the left face is

$$h \int_0^\delta \rho u^2\, dy = \rho_1 u_1^2 h (\delta - \delta^* - \vartheta) \quad ,$$

while the momentum carried out through the right face is

$$\rho_1 u_1^2 h (\delta - \delta^* - \vartheta) + dx \frac{\partial}{\partial x}\left\{\rho_1 u_1^2 h (\delta - \delta^* - \vartheta)\right\} .$$

The net momentum change through these faces is then

$$dx \frac{\partial}{\partial x}\left\{\rho_1 u_1^2 h (\delta - \delta^* - \vartheta)\right\} .$$

Similarly, the mass entering the left face is

$$h\int_0^{\delta} \rho u \, dy = \rho_1 u_1 h (\delta - \delta^*)$$

and that leaving the right face is

$$\rho_1 u_1 h (\delta - \delta^*) + dx \frac{\partial}{\partial x}\left\{\rho_1 u_1 h (\delta - \delta^*)\right\} .$$

From continuity considerations, the mass increment leaving the right face must have entered through the top of the element, and this mass carries in with it a momentum equal to

$$u_1 \, dx \frac{\partial}{\partial x}\left\{\rho_1 u_1 h (\delta - \delta^*)\right\} .$$

The net momentum change from all faces becomes

$$-dx \frac{\partial}{\partial x}\left\{\rho_1 u_1^2 h (\delta - \delta^* - \vartheta)\right\} + u_1 \, dx \frac{\partial}{\partial x}\left\{\rho_1 u_1 h (\delta - \delta^*)\right\}$$

$$= -dx \frac{\partial}{\partial x}\left\{\rho_1 u_1^2 h (\delta - \delta^* - \vartheta - \delta + \delta^*)\right\} + \rho_1 u_1 h (\delta - \delta^*) \frac{\partial u_1}{\partial x} dx$$

$$= -dx \frac{\partial}{\partial x}(\rho_1 u_1^2 h \vartheta) + \rho_1 u_1 h \delta \frac{\partial u_1}{\partial x} dx - \rho_1 u_1 h \delta^* \frac{\partial u_1}{\partial x} dx .$$

Equating momentum change to forces and eliminating dx results in the equation

$$h\tau_o + h\delta \frac{\partial p}{\partial x} = \frac{\partial}{\partial x}(\rho_1 u_1^2 h \vartheta) - \rho_1 u_1 h \delta \frac{\partial u_1}{\partial x} + \rho_1 u_1 h \delta^* \frac{\partial u_1}{\partial x} \qquad (5)$$

The pressure term can be eliminated by reference to the one-dimensional momentum relation

$$u_1 du_1 + \frac{dp}{\rho_1} = 0 \quad ,$$

so that

$$\frac{dp}{dx} = -\rho_1 u_1 \frac{du_1}{dx} \quad .$$

With this substitution, equation (5) reduces to the basic equation for the boundary layer

$$h\tau_o = \frac{d}{dx}(\rho_1 u_1^2 h \vartheta) + \rho_1 u_1 h \delta^* \frac{du_1}{dx} \quad , \qquad (6)$$

where total derivatives are utilized, since the quantities considered are functions only of x. Introducing the relation

$$\tau_o = \tfrac{1}{2} c_f \rho_1 u_1^2 \qquad (7)$$

equation (6) transforms into

$$\tfrac{1}{2} c_f = \frac{1}{\rho_1 u_1^2 h} \frac{d}{dx}(\rho_1 u_1^2 h \vartheta) + \frac{\delta^*}{u_1} \frac{du_1}{dx}$$

or

$$\tfrac{1}{2} c_f = \frac{d\vartheta}{dx} + \frac{\vartheta}{\rho_1 u_1^2} \frac{d}{dx}(\rho_1 u_1^2) + \frac{\vartheta}{h} \frac{dh}{dx} + \frac{\delta^*}{u_1} \frac{du_1}{dx} \qquad (8)$$

Utilizing the one-dimensional relation

$$\frac{d}{dx}(\rho_1 u_1^2) = \rho_1 u_1 (2 - M_1^2) \frac{du_1}{dx}$$

equation (8) becomes,

$$\frac{1}{2} C_f = \frac{d\vartheta}{dx} + \frac{\vartheta}{u_1}(2 - M_1^2) \frac{du_1}{dx} + \frac{\vartheta}{h} \frac{dh}{dx} + \frac{\delta^*}{u_1} \frac{du_1}{dx} \quad . \tag{9}$$

At this point, the assumption of an invariant velocity profile is introduced, where the velocity variation through the boundary layer is given in the dimensionless form

$$\omega = \omega(\eta) \qquad \omega \equiv \frac{u}{u_1} \qquad \eta \equiv \frac{y}{\delta} \quad . \tag{10}$$

Similarly, dimensionless functions of the momentum and displacement thicknesses can be defined respectively by

$$A(M) = \frac{\vartheta}{\delta} \tag{11}$$

and

$$B(M) = \frac{\delta^*}{\delta} \tag{12}$$

where the notation indicates their dependence only upon the Mach number of the potential flow for an invariant velocity profile. All subsequent functions of the boundary layer will similarly be expressed in terms of the Mach number of the potential flow.

Introducing these functions, equation (9) becomes

$$\frac{1}{2} C_f = A \frac{d\delta}{dx} + \delta \frac{dA}{dx} + \frac{A}{u_1}(2 - M_1^2) \frac{du_1}{dx} + \frac{B\delta}{u_1} \frac{du_1}{dx} + \frac{A\delta}{h} \frac{dh}{dx}$$

or

$$\frac{c_f}{2A} = \frac{d\delta}{dx} + \frac{\delta}{Au_1}\frac{du_1}{dx}\left[(2-M_1^2)A + B + u_1\frac{dA}{du_1}\right] + \frac{\delta}{h}\frac{dh}{dx} \quad . \tag{13}$$

Defining additional functions by

$$C(M) = u_1 \frac{d}{du_1} A(M) \tag{14}$$

$$D(M) = (2 - M_1)\, A(M) + B(M) + C(M), \tag{15}$$

equation (13) becomes

$$\frac{c_f}{2A} = \frac{d\delta}{dx} + \delta\left\{\frac{D}{Au_1}\frac{du_1}{dx} + \frac{1}{h}\frac{dh}{dx}\right\} \tag{16}$$

which can be recognized as a first order linear differential equation, and thus has the solution

$$\delta = \frac{1}{G(M_x)H(M_x)}\left\{\int_0^x \frac{G(M)H(M)}{A(M)}\frac{c_f}{2}\,dx + \delta_t\right\} \tag{17}$$

where

$$G(M) = e^{\int \frac{D(M)}{A(M)}\frac{du_1}{u_1}} \tag{18}$$

and

$$H(M) = e^{\int \frac{dh}{h}} \quad . \tag{19}$$

The integrations indicated in equations (17), (18), and (19) are all from the nozzle throat down to the station in question, and δ_t accordingly represents the boundary layer thickness at the throat. In practically all cases, the fluid acceleration in the contraction section ahead of the throat is so high that δ_t is very small and can safely be neglected.

Inserting the limits of integration into equation (19), it is seen that H(M) can immediately be integrated as follows

$$H(M) = e^{\int_{h^*}^{h} \frac{dh}{h}} = e^{\log \frac{h}{h^*}} = \frac{h}{h^*} = \frac{h}{h^*}(M) \quad , \tag{20}$$

with the result that H(M) represents simply the wall height ratio or, in the case of one of the parallel walls of a two-dimensional channel, the area ratio between the station in question and the throat.

Introducing this value of H(M) into equation (17), and neglecting δ_t, the total boundary layer thickness is given by

$$\delta_x = \frac{1}{G(M)} \frac{h^*}{h} \int_0^x \frac{h}{h^*} \cdot \frac{G(M)}{A(M)} \frac{C_f}{2} dx \tag{21}$$

However, the total thickness is of importance only as a means of determining the displacement thickness, δ^*, upon which the nozzle design is based. Remembering that

$$\delta^* = \delta \cdot B(M) \tag{12}$$

the displacement thickness can be obtained from

$$\delta_x^* = \frac{h^*}{h} \frac{B(M)}{G(M)} \int_0^x \frac{h}{h^*} \frac{G(M)}{A(M)} \frac{C_f}{2} dx \quad . \tag{22}$$

Equation (22) is still general to the extent that the friction coefficient can be a function of position along the nozzle length. However, insufficient information is available with which to predict this variation of C_f with any accuracy, thus it is necessary here to remove it from under the integral sign and assign an average or effective value for the nozzle as a whole. It is hoped that sufficient experimental results can be obtained to determine this effective C_f value as a function of Reynolds number and Mach number. From Reynolds number considerations alone, this value can be expected to lie in the range from 0.001 to 0.003 for the usual supersonic wind tunnel size (Ref. 6).

With this change, the final equation for the displacement thickness is

$$\delta_x^* = \frac{1}{2} C_f \frac{h^*}{h} \frac{B(M)}{G(M)} \int_0^x \frac{h}{h^*} \frac{G(M)}{A(M)} dx \qquad (23)$$

It must be emphasized here that the factor $\frac{h}{h^*}$ appearing in this equation refers to the potential height ratio for the wall upon which the boundary layer growth is being calculated. That is, for two-dimensional channel having parallel side walls, the factor $\frac{h}{h^*}$ has the value unity for the top and bottom walls. For the side walls, in this case, the factor can be evaluated from the potential nozzle ordinates; or if more convenient, it can be taken as equal to the area ratio corresponding to the local Mach number of the potential flow.

Equation (23) is also valid for an axially symmetric nozzle so long as the boundary layer thickness is small compared with the cross-section radius. For an axially symmetric nozzle, the factor $\frac{h}{h^*}$ can be replaced by its equivalent $\frac{r}{r^*}$, resulting in

$$\delta_x^* = \tfrac{1}{2} C_f \frac{r^*}{r} \frac{B(M)}{G(M)} \int_0^x \frac{r}{r^*} \frac{G(M)}{A(M)} dx \quad . \tag{24}$$

The displacement thickness at any station along the nozzle length can be found from equations (23) or (24) by a numerical or graphical integration from the nozzle throat to the station in question, provided $\frac{h}{h^*}$ or $\frac{r}{r^*}$, $\frac{B(M)}{G(M)}$ and $\frac{G(M)}{A(M)}$ are known functions of the nozzle length. These are known if either the centerline Mach number or wall Mach number variation with nozzle length is given. The difference of these two Mach number variations is negligible in view of the other approximations inherent in this analysis.

If it is desired to incorporate a length of channel following the nozzle exit in which the Mach number is held constant, the actual channel walls must diverge sufficiently to compensate for the continued growth of boundary layer. With no axial Mach number gradient, there is of course no velocity nor pressure gradient, thus equation (8) reduces to the exceedingly simple form

$$\tfrac{1}{2} C_f = \frac{d\delta}{dx} \quad . \tag{25}$$

The $\frac{dh}{dx}$ term vanishes as well, since h refers to the potential wall height rather than the actual wall height, the difference in heights being due to the boundary layer clinging to the top and bottom walls. Actually, this simplicity is just a manifestation of the inherent simplicity of the momentum approach to the boundary layer, for equation (25) states that, in the absence of a pressure gradient, the momentum loss just balances the wall friction.

Introducing the displacement thickness, equation (25) becomes

$$\tfrac{1}{2} C_f = \frac{d\theta}{d\delta}\frac{d\delta}{d\delta^*}\frac{d\delta^*}{dx} = \frac{A(M)}{B(M)}\frac{d\delta^*}{dx}$$

so that

$$\frac{d\delta^*}{dx} = \tfrac{1}{2} C_f \frac{B(M)}{A(M)} \quad , \tag{26}$$

which is an indication of how much the physical walls must diverge in order to maintain a uniform potential shape and thus a constant Mach number.

With no Mach number gradient in the x-direction, equation (23) will of course reduce to this same form:

$$\delta_x^* = \tfrac{1}{2} C_f \frac{h^*}{h}\frac{B(M)}{G(M)} \int_0^x \frac{h}{h^*}\frac{G(M)}{A(M)}\, dx \tag{23}$$

$$\frac{d\delta^*}{dx} = \tfrac{1}{2} C_f \frac{h^*}{h}\frac{B(M)}{G(M)}\frac{\partial}{\partial x}\int_0^x \frac{h}{h^*}\frac{G(M)}{A(M)}\, dx$$

$$\frac{d\delta^*}{dx} = \tfrac{1}{2} C_f \frac{h^*}{h}\cdot\frac{B(M)}{G(M)}\cdot\frac{h}{h^*}\cdot\frac{G(M)}{A(M)}$$

$$\frac{d\delta^*}{dx} = \tfrac{1}{2} C_f \frac{B(M)}{A(M)} \quad . \tag{26}$$

The solutions to equations (23), (24) or (26) provide the information from which to determine the modification to the potential nozzle shape, but first the various functions involved must be evaluated; this is done in the next two sections.

B. Development of the General Functions

The functions A(M), B(M), C(M), D(M) and G(M) can be expressed in more convenient form if a normalized velocity "n" is utilized where the theoretical maximum velocity obtainable by isentropic expansion into a vacuum is assigned the value unity. This dimensionless normalized velocity is related to the other velocities in the fluid through the expressions:

$$n^2 = \left(\frac{u_1}{c}\right)^2 = \frac{\gamma-1}{\gamma+1}\left(\frac{u_1}{a^*}\right)^2 = \frac{\gamma-1}{2}\left(\frac{u_1}{a_o}\right)^2$$

$$M^2 = \frac{\frac{2}{\gamma-1}n^2}{1-n^2} = \frac{5n^2}{1-n^2} \qquad (27)$$

$$\frac{1}{1-n^2} = 1 + \frac{\gamma-1}{2}M^2$$

Due to the assumptions of no heat transfer to the wall, no pressure gradient normal to the wall, and a Prandtl number of unity, the density variation inversely matches the temperature variation through the boundary layer, and each recovers its stagnation value at the wall. Consequently, the density ratio can be expressed in terms of n

$$\frac{\rho}{\rho_1} = \frac{T_1}{T} = \frac{T_1/T_o}{T/T_o} = \frac{1-\left(\frac{u_1}{c}\right)^2}{1-\left(\frac{u}{c}\right)^2} = \frac{1-n^2}{1-\omega^2 n^2} \qquad (28)$$

since

$$\frac{T}{T_o} = 1-\left(\frac{u}{c}\right)^2 \quad , \quad \omega = \frac{u}{u_1}$$

With these relations, the various functions become

$$A(M) = \frac{\vartheta}{\delta} = \frac{1}{\delta}\int_0^{\delta} \frac{\rho u}{\rho_1 u_1}\left(1 - \frac{u}{u_1}\right) dy = (1-n^2)\int_0^1 \frac{\omega(1-\omega)}{1-n^2\omega^2}\, d\eta \qquad (29)$$

$$B(M) = \frac{\delta^*}{\delta} = \frac{1}{\delta}\int_0^{\delta}\left(1 - \frac{\rho u}{\rho_1 u_1}\right) dy = \int_0^1 d\eta - \int_0^1 \left(\frac{1-n^2}{1-n^2\omega^2}\right)\omega\, d\eta$$

$$B(M) = 1 - (1-n^2)\int_0^1 \frac{\omega}{1-n^2\omega^2}\, d\eta \qquad (30)$$

Utilizing the additional relation

$$\frac{du}{dM} = \frac{u}{M\left(1 + \frac{\gamma-1}{2}M^2\right)} = \frac{u}{M}(1-n^2)$$

the function C(M) can be written as

$$C(M) = u_1 \frac{dA}{du_1} = u_1 \frac{dM_1}{du_1}\frac{dA}{dM_1}$$

or

$$C(M) = \frac{M}{(1-n^2)}\frac{dA}{dM_1} = n\frac{dA}{dn}$$

Now

$$\frac{dA}{dM} = \frac{d}{dM}\left\{(1-n^2)\int_0^1 \frac{\omega(1-\omega)}{1-n^2\omega^2}\, d\eta\right\}$$

$$\frac{dA}{dM} = \left\{\int_0^1 \frac{\omega(1-\omega)}{1-n^2\omega^2}\, d\eta\right\}\frac{d}{dM}(1-n^2) + (1-n^2)\int_0^1 \frac{d}{dM}\left\{\frac{\omega(1-\omega)}{1-n^2\omega^2}\right\} d\eta$$

$$\frac{d}{dM}(1-n^2) = \frac{d}{dM}\left(1+\frac{\gamma-1}{2}M^2\right)^{-1} = \frac{-(\gamma-1)M}{\left(1+\frac{\gamma-1}{2}M^2\right)^2}$$

$$\frac{d}{dM}(1-n^2) = -(\gamma-1)M(1-n^2)^2$$

$$\frac{d}{dM}\left\{\frac{\omega(1-\omega)}{1-n^2\omega^2}\right\} = \frac{-\omega(1-\omega)}{(1-n^2\omega^2)^2}\frac{d}{dM}(1-n^2\omega^2)$$

$$\frac{d}{dM}(1-n^2\omega^2) = \omega^2\frac{d}{dM}(1-n^2) = -(\gamma-1)M\omega^2(1-n^2)^2 .$$

Combining all these derivatives

$$C(M) = -\frac{(\gamma-1)M^2(1-n^2)^2}{1-n^2}\left[\int_0^1 \frac{\omega(1-\omega)}{1-n^2\omega^2}d\eta + (1-n^2)\int_0^1 \frac{-\omega^3(1-\omega)}{(1-n^2\omega^2)^2}d\eta\right]$$

replacing

$$(\gamma-1)M^2 = \frac{2n^2}{1-n^2}$$

$$C(M) = 2n^2\left[\int_0^1 \frac{-\omega(1-\omega)}{1-n^2\omega^2}d\eta + (1-n^2)\int_0^1 \frac{\omega^3(1-\omega)}{(1-n^2\omega^2)^2}d\eta\right]$$

$$= 2n^2\int_0^1 \frac{-\omega(1-\omega)(1-n^2\omega^2) + (1-n^2)(1-\omega)\omega^3}{(1-n^2\omega^2)^2}d\eta$$

$$= 2n^2\int_0^1 \frac{-\omega(1-\omega)+\omega(1-\omega)n^2\omega^2+\omega^3(1-\omega)-n^2\omega^3(1-\omega)}{(1-n^2\omega^2)^2}d\eta$$

resulting in

$$C(M) = 2n^2 \int_0^1 \frac{\omega(1-\omega)(\omega^2-1)}{(1-n^2\omega^2)^2}\, d\eta \tag{31}$$

Similarly

$$(2-M_1^2)A(M) = \left(2 - \frac{5n^2}{1-n^2}\right)(1-n^2)\int_0^1 \frac{\omega(1-\omega)}{1-n^2\omega^2}\, d\eta$$

$$(2-M_1^2)A(M) = (2-7n^2)\int_0^1 \frac{\omega(1-\omega)}{1-n^2\omega^2}\, d\eta \tag{32}$$

so that

$$D(M) = (2-M_1^2)A(M) + B(M) + C(M) \tag{33}$$

$$D(M) = (2-7n^2)\int_0^1 \frac{\omega(1-\omega)}{1-n^2\omega^2}\, d\eta + 1$$

$$-(1-n^2)\int_0^1 \frac{\omega}{1-n^2\omega^2}\, d\eta + 2n^2 \int_0^1 \frac{\omega(1-\omega)(\omega^2-1)}{(1-n^2\omega^2)^2}\, d\eta \tag{33}$$

and

$$G(M) = e^{\int \frac{D(M)}{A(M)} \frac{du}{u_1}} = e^{\int \frac{D(M)}{A(M)} \frac{dM}{M\left(1+\frac{\gamma-1}{2}M^2\right)}} \tag{34}$$

To obtain numerical values of these functions, it is necessary to have an explicit relation between ω and η, which defines the

velocity profile. This choice of profile should be reasonably close to that expected to occur under the circumstances, and of course it must be simple enough to be integrable. These two considerations greatly restrict the choice of a velocity profile. As a result, only two profiles have been completely evaluated:

1) Linear velocity profile $(\omega = \eta)$

2) Turbulent velocity profile $(\omega = \eta^{\frac{1}{7}})$

Based on these two velocity profiles, numerical values of the boundary layer functions are obtained in the next section.

C. Evaluation of Linear Velocity Profile Functions

The linear velocity profile represents the simplest form to evaluate. For this profile

$$\omega = \eta \qquad \text{so that} \qquad d\omega = d\eta \tag{35}$$

and the functions can easily be integrated.

$$A(M) = (1-n^2)\int_0^1 \frac{\omega(1-\omega)}{1-n^2\omega^2}\,d\omega = (1-n^2)\int_0^1 \frac{\omega\,d\omega}{1-n^2\omega^2} - (1-n^2)\int_0^1 \frac{\omega^2 d\omega}{1-n^2\omega^2}$$

$$= \frac{1-n^2}{-2n^2}\log(1-n^2) + \frac{1-n^2}{n^2} - \frac{1-n^2}{2n^3}\log\frac{1+n}{1-n}$$

$$A(M) = \frac{1}{\frac{\gamma-1}{2}M^2}\left[1 + \log\sqrt{1+\tfrac{\gamma-1}{2}M^2} + \sqrt{\frac{2}{(\gamma-1)M^2}+1}\,\log\left(\sqrt{1+\tfrac{\gamma-1}{2}M^2} - \sqrt{\tfrac{\gamma-1}{2}M^2}\right)\right] \tag{36}$$

$$B(M) = 1 - (1-n^2)\int_0^1 \frac{\omega\, d\omega}{1-n^2\omega^2} = 1 + \frac{1-n^2}{2n^2}\log(1-n^2)$$

$$B(M) = 1 - \frac{1}{\frac{\gamma-1}{2}M^2}\log\sqrt{1+\frac{\gamma-1}{2}M^2} \qquad (37)$$

$$C(M) = 2n^2\int_0^1 \frac{\omega(1-\omega)(\omega^2-1)}{(1-n^2\omega^2)^2}\,d\omega = n\frac{dA}{dn}$$

$$C(M) = -2n^2\int_0^1 \frac{(\omega^4-\omega^3-\omega^2+\omega)}{(1-n^2\omega^2)^2}\,d\omega = -2n^2\left(I_1 - I_2 - I_3 + I_4\right)$$

Considering each of these four integrals separately

$$I_1 = \int_0^1 \frac{\omega^4\, d\omega}{(1-n^2\omega^2)^2} = -\frac{1}{n^2}\int_0^1 \frac{\omega^2\, d\omega}{1-n^2\omega^2} + \frac{1}{n^2}\int_0^1 \frac{\omega^2\, d\omega}{(1-n^2\omega^2)^2} = \frac{1}{n^2}\left(-I_5 + I_6\right)$$

I_5 appears in A(M) above so is already evaluated

$$I_6 = \int_0^1 \frac{\omega^2\, d\omega}{(1-n^2\omega^2)^2} = -\frac{1}{n^2}\int_0^1 \frac{d\omega}{1-n^2\omega^2} + \frac{1}{n^2}\int_0^1 \frac{d\omega}{(1-n^2\omega^2)^2} = \frac{1}{n^2}\left(I_7 + I_8\right)$$

$$I_7 = \int_0^1 \frac{d\omega}{1-n^2\omega^2} = \frac{1}{2n}\log\frac{1+n}{1-n}$$

$$I_8 = \int_0^1 \frac{d\omega}{(1-n^2\omega^2)^2} = \frac{1}{2(1-n^2)} + \frac{1}{2}\int_0^1 \frac{d\omega}{1-n^2\omega^2} = \frac{1}{2(1-n^2)} + \frac{1}{4n}\log\frac{1+n}{1-n}$$

$$I_2 = \int_0^1 \frac{\omega^3\, d\omega}{(1-n^2\omega^2)^2} = -\frac{1}{n^2}\int_0^1 \frac{\omega\, d\omega}{1-n^2\omega^2} + \frac{1}{n^2}\int_0^1 \frac{\omega\, d\omega}{(1-n^2\omega^2)^2} = \frac{1}{n^2}\left(-I_9 + I_{10}\right)$$

Again, I_9 appears in A(M) and has been evaluated.

$$I_{10} = \int_0^1 \frac{\omega\, d\omega}{(1-n^2\omega^2)^2} = \frac{1}{2n^2(1-n^2)} - \frac{1}{2n^2} = \frac{1-(1-n^2)}{2n^2(1-n^2)} = \frac{1}{2(1-n^2)}$$

$$I_3 = \int_0^1 \frac{\omega^2\, d\omega}{(1-n^2\omega^2)^2} = I_6$$

$$I_4 = \int_0^1 \frac{\omega\, d\omega}{(1-n^2\omega^2)^2} = I_{10}$$

Combining all these integrals

$$C(M) = -2n^2\left[\frac{1}{n^2}\left(-I_5 + I_6 + I_9 - I_{10}\right) - I_6 + I_{10}\right]$$

$$C(M) = -2\left(I_9 - I_5\right) + 2(1-n^2)\left(I_{10} - I_6\right)$$

$$A(M) = \left(1-n^2\right)\left(I_9 - I_5\right) \qquad B(M) = 1 - (1-n^2)I_9$$

$$C(M) = -\frac{2}{1-n^2}A(M) + 2(1-n^2)\left(I_{10} - I_6\right)$$

$$= -\frac{2}{1-n^2}A(M) + 2(1-n^2)\left[\frac{1}{2(1-n^2)} - \frac{1}{2n^2(1-n^2)} + \frac{1}{4n^3}\log\frac{1+n}{1-n}\right]$$

$$= -\frac{2}{1-n^2}A(M) + \frac{1-n^2}{n^2} + \frac{1-n^2}{2n^3}\log\frac{1+n}{1-n}$$

$$A(M) = \frac{1-n^2}{n^2} + \frac{1-n^2}{2n^3}\log\frac{1+n}{1-n} + B(M) - 1$$

which can simplify C(M) still further to

$$C(M) = -\frac{2}{1-n^2}A(M) - A(M) - B(M) + 1$$

$$= \left(-2 - \{\gamma-1\}M^2 - 1\right)A(M) - B(M) + 1$$

$$C(M) = -\left(3 + \gamma M^2 - M^2\right) A(M) - B(M) + 1 \tag{38}$$

$$D(M) = \left(2 - M^2\right) A(M) + B(M) + C(M)$$

$$D(M) = 1 - \left(1 + \gamma M^2\right) A(M) \tag{39}$$

$$G(M) = e^{\int \frac{D(M)}{A(M)} \frac{du_1}{u_1}} = e^{\int \left(\frac{1}{A(M)} - 1 - \gamma M^2\right) \frac{dM}{M\left(1 + \frac{\gamma - 1}{2} M^2\right)}} \tag{40}$$

Of these linear profile functions, only G(M) requires a numerical or graphical integration for its evaluation. Curves of these functions are given in Figures 2 to 11.

D. Evaluation of 1/7 Power Velocity Profile Functions

If the velocity profile is assumed to vary as the seventh root of the distance from the wall, the dimensionless relation expressing this is

$$\omega = \eta^{\frac{1}{7}} \qquad \text{so that} \qquad d\eta = 7\omega^6 d\omega \tag{41}$$

and the several functions become

$$A(M) = \frac{\delta}{\delta} = \left(1 - n^2\right) \int_0^1 \frac{7\omega^7 (1 - \omega)}{1 - n^2 \omega^2} d\omega \tag{42}$$

$$B(M) = \frac{\delta^*}{\delta} = 1 - \left(1 - n^2\right) \int_0^1 \frac{7\omega^7}{1 - n^2 \omega^2} d\omega \tag{43}$$

$$C(M) = u_1 \frac{dA}{du_1} = 14n^2 \int_0^1 \frac{\omega^7(1-\omega)(\omega^2-1)}{(1-n^2\omega^2)^2} d\omega \qquad (44)$$

in which it is remembered that M is a function of n. The evaluation of A(M) in closed form proceeds as follows:

$$A(M) = (1-n^2)\int_0^1 \frac{\omega^7 d\omega}{1-n^2\omega^2} - (1-n^2)\int_0^1 \frac{\omega^8 d\omega}{1-n^2\omega^2} = (1-n^2)(I_{1A} - I_{2A})$$

$$I_{1A} = \int_0^1 \frac{\omega^7 d\omega}{1-n^2\omega^2} = -\frac{1}{n^2}\int_0^1 \omega^5 d\omega + \frac{1}{n^2}\int_0^1 \frac{\omega^5 d\omega}{1-n^2\omega^2} = -\frac{1}{6n^2} + \frac{1}{n^2} I_{3A}$$

$$I_{3A} = \int_0^1 \frac{\omega^5 d\omega}{1-n^2\omega^2} = -\frac{1}{n^2}\int_0^1 \omega^3 d\omega + \frac{1}{n^2}\int_0^1 \frac{\omega^3 d\omega}{1-n^2\omega^2} = -\frac{1}{4n^2} + \frac{1}{n^2} I_{4A}$$

$$I_{4A} = \int_0^1 \frac{\omega^3 d\omega}{1-n^2\omega^2} = -\frac{1}{n^2}\int_0^1 \omega\, d\omega + \frac{1}{n^2}\int_0^1 \frac{\omega\, d\omega}{1-n^2\omega^2} = -\frac{1}{2n^2} + \frac{1}{2n^2}\,\frac{\log(1-n^2)}{n^2}$$

$$I_{1A} = -\frac{1}{6n^2} - \frac{1}{4n^4} - \frac{1}{2n^6} - \frac{1}{2n^8}\log(1-n^2)$$

$$I_{2A} = \int_0^1 \frac{\omega^8 d\omega}{1-n^2\omega^2} = -\frac{1}{n^2}\int_0^1 \omega^6 d\omega + \frac{1}{n^2}\int_0^1 \frac{\omega^6 d\omega}{1-n^2\omega^2} = -\frac{1}{7n^2} + \frac{1}{n^2} I_{5A}$$

$$I_{5A} = \int_0^1 \frac{\omega^6 d\omega}{1-n^2\omega^2} = -\frac{1}{n^2}\int_0^1 \omega^4 d\omega + \frac{1}{n^2}\int_0^1 \frac{\omega^4 d\omega}{1-n^2\omega^2} = -\frac{1}{5n^2} + \frac{1}{n^2} I_{6A}$$

$$I_{6A} = \int_0^1 \frac{\omega^4 d\omega}{1-n^2\omega^2} = -\frac{1}{n^2}\int_0^1 \omega^2 d\omega + \frac{1}{n^2}\int_0^1 \frac{\omega^2 d\omega}{1-n^2\omega^2} = -\frac{1}{3n^2} + \frac{1}{n^2} I_{7A}$$

$$I_{7A} = \int_0^1 \frac{\omega^2 d\omega}{1-n^2\omega^2} = -\frac{1}{n^2}\int_0^1 d\omega + \frac{1}{n^2}\int_0^1 \frac{d\omega}{1-n^2\omega^2} = -\frac{1}{n^2} + \frac{1}{n^2} I_{8A}$$

$$I_{8A} = \int_0^1 \frac{d\omega}{1-n^2\omega^2} = \frac{1}{2n}$$

$$I_{2A} = -\frac{1}{7n^2} - \frac{1}{5n^4} - \frac{1}{3n^6} - \frac{1}{n^8} + \frac{1}{2n^9}\log\frac{1+n}{1-n}$$

Collecting these integrals

$$A(M) = 7(1-n^2)(I_{1A} - I_{2A})$$

$$= 7(1-n^2)\left(\frac{1}{7n^2} - \frac{1}{6n^2} + \frac{1}{5n^4} - \frac{1}{4n^4} + \frac{1}{3n^6} - \frac{1}{2n^6} + \frac{1}{n^8} - \frac{1}{2n^8}\log(1-n^2) - \frac{1}{2n^9}\log\frac{1+n}{1-n}\right)$$

$$= 7(1-n^2)\left(-\frac{1}{42n^2} - \frac{1}{20n^4} - \frac{1}{6n^6} + \frac{1}{n^8} - \frac{1}{2n^8}\log(1-n^2) - \frac{1}{2n^9}\log\frac{1+n}{1-n}\right)$$

$$A(M) = \frac{7}{2}\frac{(1-n^2)}{n^8}\left[2 - \frac{n^2}{3} - \frac{n^4}{10} - \frac{n^6}{21} - \log(1-n^2) - \frac{1}{n}\log\frac{1+n}{1-n}\right] \qquad (45)$$

This form turns out to be inconvenient for computations, so an alternate expression can be developed in infinite series form. Expressing A(M) again in the form

$$A(M) = 7(1-n^2)(I_{1A} - I_{2A})$$

where

$$I_{1A} = -\frac{1}{2n^8}\left\{\log(1-n^2) + n^2 + \frac{n^4}{2} + \frac{n^6}{3}\right\}$$

and

$$I_{2A} = \frac{1}{2n^9}\left\{\log\left(\frac{1+n}{1-n}\right) - 2\left(n + \frac{n^3}{3} + \frac{n^5}{5} + \frac{n^7}{7}\right)\right\} \quad ,$$

the logarithmic terms can be expanded in convergent infinite series:

$$\log(1-n^2) = -\left(n^2 + \frac{n^4}{2} + \frac{n^6}{3} + \frac{n^8}{4} + \cdots\right) = -\sum_{s=1}^{\infty} \frac{n^{2s}}{s}$$

$$\log\left(\frac{1+n}{1-n}\right) = 2\left(n + \frac{n^3}{3} + \frac{n^5}{5} + \frac{n^7}{7} + \cdots\right) = \sum_{t=1}^{\infty} \frac{n^{2t-1}}{2t-1}$$

Note that these cancel exactly the other terms in I_{1A} and I_{2A}, leaving

$$I_{1A} = -\frac{1}{2n^8}\left\{\frac{n^8}{4} + \frac{n^{10}}{5} + \frac{n^{12}}{6} + \cdots\right\} = -\frac{1}{2n^8}\sum_{s=4}^{\infty} \frac{n^{2s}}{s}$$

$$I_{2A} = \frac{1}{n^9}\left\{\frac{n^9}{9} + \frac{n^{11}}{11} + \frac{n^{13}}{13} + \cdots\right\} = \frac{1}{n^9}\sum_{s=4}^{\infty} \frac{n^{2s+1}}{2s+1}$$

Combining the integrals

$$I_{1A} - I_{2A} = -\sum_{s=0}^{\infty} \frac{n^{2s}}{8+2s} + \sum_{s=0}^{\infty} \frac{n^{2s}}{9+2s} = \sum_{s=0}^{\infty} \frac{n^{2s}}{(8+2s)(9+2s)}$$

so that the solution for A(M) becomes

$$A(M) = 7(1-n^2)\sum_{s=0}^{\infty} \frac{n^{2s}}{(8+2s)(9+2s)} \qquad (46)$$

If A(M) is approximated by the finite series

$$A(M) = 7(1-n^2) \sum_{s=0}^{m} \frac{n^{2s}}{(8+2s)(9+2s)} \quad , \tag{47}$$

the accuracy of the result depends upon the size of the remainder, or tail of the series, which has been neglected. This remainder R is equal to

$$\mathcal{R} = 7(1-n^2) \sum_{s=m+1}^{\infty} \frac{n^{2s}}{(8+2s)(9+2s)} = 7(1-n^2) \sum_{s=m+1}^{\infty} a_s$$

where

$$a_s = \frac{n^{2s}}{(8+2s)(9+2s)} \quad .$$

Remembering that n is always less than unity, an inequality for R can be obtained as

$$\mathcal{R} < 7(1-n^2) \sum_{s=0}^{\infty} a_{m+1} n^{2s} = 7(1-n^2) \frac{a_{m+1}}{(1-n^2)} = 7 a_{m+1} \quad .$$

Thus the remainder term is always less than seven times the first term omitted.

The inequality can also be given that the remainder is less than $7n^2$ times the last term considered; this follows from the fact that

$$a_{m+1} = \frac{(8+2m)(9+2m)}{(10+2m)(11+2m)} a_m n^2 < a_m n^2 \quad .$$

The function B(M) can be evaluated in similiar fashion:

$$B(M) = 1 - (1-n^2) \int_0^1 \frac{7\omega^7 d\omega}{1-n^2\omega^2} = 1 - 7(1-n^2) I_{1B}$$

where this integral I_{1B} is the same as for A(M), $I_{1B} = I_{1A}$.

Thus

$$B(M) = 1 + \frac{7(1-n^2)}{2n^8}\left\{\log(1-n^2) + n^2 + \frac{n^4}{4} + \frac{n^6}{6}\right\} \qquad (48)$$

or in the alternate form

$$B(M) = 1 - 7(1-n^2)\sum_{s=0}^{\infty}\frac{n^{2s}}{8+2s} \qquad (49)$$

The reduction of C(M) follows the same scheme:

$$C(M) = 14n^2\int_0^1 \frac{\omega^7(1-\omega)(\omega^2-1)}{(1-n^2\omega^2)^2}\,d\omega$$

$$= -14n^2\int_0^1 \frac{\omega^{10}-\omega^9-\omega^8+\omega^7}{(1-n^2\omega^2)^2}\,d\omega = -14n^2\left(I_{1C} - I_{2C} - I_{3C} + I_{4C}\right)$$

This integral form corresponds to form No. 125-2, page 66 of Burington's Tables of Integrals.

$$I_{1C} = \int_0^1 \frac{\omega^{10}\,d\omega}{(1-n^2\omega^2)^2} \quad \sim \int x^{m-1}(ax^n+c)^p\,dx$$

where $c = 1,\ a = -n^2,\ m = 11,\ n = 2,\ p = -2$

$$I_{1C} = \frac{1}{2(1-n^2)} - \frac{9}{2}\int_0^1 \frac{\omega^{10}}{1-n^2\omega^2}\,d\omega = \frac{1}{2(1-n^2)} - \frac{9}{2}I_{5C}$$

By comparison with integral I_{2A}, the value of I_{5C} can be obtained immediately as

$$I_{5C} = -\frac{1}{9n^2} - \frac{1}{7n^4} - \frac{1}{5n^6} - \frac{1}{3n^8} - \frac{1}{n^{10}} + \frac{1}{2n^{11}}\log\left(\frac{1+n}{1-n}\right)$$

or as

$$I_{5C} = -\frac{1}{n^{11}}\left\{\log\sqrt{\frac{1-n}{1+n}} + n + \frac{n^3}{3} + \frac{n^5}{5} + \frac{n^7}{7} + \frac{n^9}{9}\right\}$$

Similarly

$$I_{2C} = \int_0^1 \frac{\omega^9\, d\omega}{(1-n^2\omega^2)^2} = \frac{1}{2(1-n^2)} - \frac{8}{2}\int_0^1 \frac{\omega^9 d\omega}{1-n^2\omega^2} = \frac{1}{2(1-n^2)} - \frac{8}{2} I_{6C}$$

$$I_{6C} = -\frac{1}{2n^{10}}\left\{\log(1-n^2) + n^2 + \frac{n^4}{2} + \frac{n^6}{3} + \frac{n^8}{4}\right\}$$

$$I_{3C} = \int_0^1 \frac{\omega^8\, d\omega}{(1-n^2\omega^2)^2} = \frac{1}{2(1-n^2)} - \frac{7}{2}\int_0^1 \frac{\omega^8 d\omega}{1-n^2\omega^2} = \frac{1}{2(1-n^2)} - \frac{7}{2} I_{7C}$$

$$I_{7C} \equiv I_{2A} = -\frac{1}{n^9}\left\{\log\sqrt{\frac{1-n}{1+n}} + n + \frac{n^3}{3} + \frac{n^5}{5} + \frac{n^7}{7}\right\}$$

$$I_{4C} = \int_0^1 \frac{\omega^7\, d\omega}{(1-n^2\omega^2)^2} = \frac{1}{2(1-n^2)} - \frac{6}{2}\int_0^1 \frac{\omega^7 d\omega}{1-n^2\omega^2} = \frac{1}{2(1-n^2)} - \frac{6}{2} I_{8C}$$

$$I_{8C} \equiv I_{1A} = -\frac{1}{2n^8}\left\{\log(1-n^2) + n^2 + \frac{n^4}{2} + \frac{n^6}{3}\right\}$$

Summing up these integrals

$$I_{1C} - I_{2C} - I_{3C} + I_{4C} = -\frac{9}{2} I_{5C} + \frac{8}{2} I_{6C} + \frac{7}{2} I_{7C} - \frac{6}{2} I_{8C}$$

$$C(M) = 7n^2\left[9 I_{5C} - 8 I_{6C} - 7 I_{7C} + 6 I_{8C}\right]$$

$$\frac{C(M)}{7n^2} = -\frac{9}{n^{11}}\left\{\log\sqrt{\frac{1-n}{1+n}} + n + \frac{n^3}{3} + \frac{n^5}{5} + \frac{n^7}{7} + \frac{n^9}{9}\right\}$$

$$+\frac{8}{2n^{10}}\left\{\log(1-n^2) + n^2 + \frac{n^4}{2} + \frac{n^6}{3} + \frac{n^8}{4}\right\}$$

$$+\frac{7}{n^9}\left\{\log\sqrt{\frac{1-n}{1+n}} + n + \frac{n^3}{3} + \frac{n^5}{5} + \frac{n^7}{7}\right\}$$

$$-\frac{6}{2n^8}\left\{\log(1-n^2) + n^2 + \frac{n^4}{2} + \frac{n^6}{3}\right\}$$

Combining coefficients

$$\frac{C(M)}{7n^2} = -\frac{9}{n^{11}}\log\sqrt{\frac{1-n}{1+n}} + \frac{1}{n^{10}}\left\{-9 + 4\log(1-n^2)\right\} + \frac{7}{n^9}\left\{\log\sqrt{\frac{1-n}{1+n}}\right\}$$

$$+\frac{1}{n^8}\left\{-3+4+7\right\} + \frac{1}{n^7}\left\{0\right\} + \frac{1}{n^6}\left\{-\frac{9}{5}+2+\frac{7}{3}-3\right\}$$

$$+\frac{1}{n^4}\left\{-\frac{9}{7}+\frac{4}{3}+\frac{7}{5}-\frac{3}{2}\right\} + \frac{1}{n^2}\left\{-1+1+1-1\right\} - \frac{3}{n^8}\log(1-n^2)$$

Finally

$$C(M) = -\frac{63}{n^9}\log\sqrt{\frac{1-n}{1+n}} + \frac{1}{n^8}\left\{-63 + 28\log(1-n^2)\right\}$$

$$+\frac{49}{n^7}\log\sqrt{\frac{1-n}{1+n}} + \frac{1}{n^6}\left\{56 - 21\log(1-n^2)\right\}$$

$$+\frac{49}{15n^4} - \frac{11}{30n^2} \qquad (50)$$

However, this expression is not amenable to accurate computation for it requires the difference of two large quantities for all values of n. As before, an alternate infinite series form is developed.

Returning to the expression

$$C(M) = 7n^2\left\{9I_{5C} - 8I_{6C} - 7I_{7C} + 6I_{8C}\right\}$$

each of these integrals can be easily evaluated in infinite series form, convergent for all values of the speed parameter n which, of course, can never reach the value unity.

$$I_{5C} = \int_0^1 \frac{\omega^{10}d\omega}{1-n^2\omega^2} = \int_0^1 \omega^{10}\left\{1 + n^2\omega^2 + n^4\omega^4 + n^6\omega^6 + \cdots\right\}d\omega$$

$$I_{5C} = \sum_{m=0}^{\infty}\int_0^1 n^{2m}\,\omega^{10+2m}\,d\omega = \sum_{m=0}^{\infty}\frac{n^{2m}}{11+2m}$$

$$I_{6C} = \int_0^1 \frac{\omega^9 d\omega}{1-n^2\omega^2} = \sum_{m=0}^{\infty}\frac{n^{2m}}{10+2m}$$

$$I_{7C} = \int_0^1 \frac{\omega^8 d\omega}{1-n^2\omega^2} = \sum_{m=0}^{\infty}\frac{n^{2m}}{9+2m}$$

$$I_{8C} = \int_0^1 \frac{\omega^7 d\omega}{1-n^2\omega^2} = \sum_{m=0}^{\infty}\frac{n^{2m}}{8+2m}$$

Combining these series

$$C(M) = 7\sum_{m=0}^{\infty} n^{2m+2}\left(\frac{9}{11+2m} - \frac{8}{10+2m} - \frac{7}{9+2m} + \frac{6}{8+2m}\right)$$

$$C(M) = \sum_{m=0}^{\infty} C_m\, n^{2m+2} \qquad (51)$$

where

$$c_m = 7\left(\frac{9}{11+2m} - \frac{8}{10+2m} - \frac{7}{9+2m} + \frac{6}{8+2m}\right)$$

which can be manipulated into a single fraction

$$\frac{1}{7}c_m = \frac{9(10+2m) - 8(11+2m)}{(11+2m)(10+2m)} + \frac{6(9+2m) - 7(8+2m)}{(9+2m)(8+2m)}$$

$$= \frac{2+2m}{(11+2m)(10+2m)} - \frac{2+2m}{(9+2m)(8+2m)}$$

$$= \frac{(2+2m)\left[(9+2m)(8+2m) - (11+2m)(10+2m)\right]}{(8+2m)(9+2m)(10+2m)(11+2m)}$$

$$= 2(1+m)\frac{-(38+8m)}{(8+2m)(9+2m)(10+2m)(11+2m)}$$

$$c_m = \frac{-28(1+m)(19+4m)}{(8+2m)(9+2m)(10+2m)(11+2m)}$$

Some of these coefficients are tabulated below:

m	C_m	m	C_m
0	0.0671717	15	0.0145617
1	0.0750583	16	0.0133390
2	0.0692308	17	0.0122622
3	0.0607843	18	0.0113092
4	0.0526746	19	0.0104621
5	0.0456140	20	0.0097059
6	0.0396574	23	0.0078682
7	0.0346772	28	0.0057852
8	0.0305128	33	0.0044261
9	0.0270164	38	0.0034954
10	0.0240638	43	0.0028298
11	0.0215543	48	0.0023374
12	0.01940731	53	0.0019630
13	0.0175587	58	0.0016717
14	0.0159573		

It should be noted here that, if A(M) is already known, C(M) can be expressed in a somewhat simpler form in terms of A(M). Remembering that

$$C(M) = n \frac{d}{dn} A(M)$$

where

$$A(M) = \frac{7}{2}\frac{1-n^2}{n^8}\left\{2 - \frac{n^2}{3} - \frac{n^4}{10} - \frac{n^6}{21} - \log(1-n^2) - \frac{1}{n}\log\left(\frac{1+n}{1-n}\right)\right\}$$

$$\frac{dA}{dn} = \frac{\left\{n^8(-2n) - 8n^7(1-n^2)\right\} n^8 A(M)}{n^{16}(1-n^2)} + \frac{7}{2}\frac{1-n^2}{n^8}\left\{-\frac{2n}{3} - \frac{4n^3}{10}\right.$$

$$\left. - \frac{6n^5}{21} - \frac{2n}{1-n^2} + \frac{1}{n^2}\log\left(\frac{1+n}{1-n}\right) - \frac{1}{n}\left(\frac{1}{1+n} - \frac{1}{1-n}\right)\right\}$$

resulting in

$$C(M) = \frac{6n^2-8}{1-n^2}A(M) - 7\frac{(1-n^2)}{9}\left\{\frac{n^3}{3} + \frac{n^5}{5}\right.$$

$$\left. + \frac{n^7}{7} - \frac{n^3}{1-n^2} + \frac{n}{1-n^2} - \frac{1}{2}\log\left(\frac{1+n}{1-n}\right)\right\} \qquad (52)$$

Using the infinite series form for A(M)

$$A(M) = 7(1-n^2)\sum_{s=0}^{\infty}\frac{n^{2s}}{(8+2s)(9+2s)}$$

$$C(M) = -14\sum_{s=0}^{\infty}\frac{n^{2s+2}}{(8+2s)(9+2s)} + 7(1-n^2)\sum_{s=0}^{\infty}\frac{n^{2s}}{2s(8+2s)(9+2s)}$$

$$C(M) = -\frac{2n^2}{1-n^2}A(M) + 7(1-n^2)\sum_{s=0}^{\infty}\frac{n^{2s}}{2s(8+2s)(9+2s)} \qquad (53)$$

Collecting these functions for the turbulent velocity profile

$$A(M) = \frac{7(1-n^2)}{2n^8}\left\{2 - \frac{n^2}{3} - \frac{n^4}{10} - \frac{n^6}{21} - \log(1-n^2) - \frac{1}{n}\log\left(\frac{1+n}{1-n}\right)\right\} \tag{45}$$

$$A(M) = 7(1-n^2)\sum_{s=0}^{\infty}\frac{n^{2s}}{(8+2s)(9+2s)} \tag{46}$$

$$B(M) = 1 + \frac{7}{2}\frac{(1-n^2)}{n^8}\left\{\log(1-n^2) + n^2 + \frac{n^4}{2} + \frac{n^6}{3}\right\} \tag{48}$$

$$B(M) = 1 - 7(1-n^2)\sum_{s=0}^{\infty}\frac{n^{2s}}{(8+2s)} \tag{49}$$

$$C(M) = -\frac{63}{n^9}\log\sqrt{\frac{1-n}{1+n}} + \left(-63 + 28\log(1-n^2)\right)n^{-8} + 49n^{-7}\log\sqrt{\frac{1-n}{1+n}}$$

$$+ n^{-6}\left\{56 - 21\log(1-n^2)\right\} + \frac{49}{15}n^{-4} - \frac{11}{30}n^{-2} \tag{50}$$

$$C(M) = -\sum_{m=0}^{\infty}\frac{28(1+m)(19+4m)}{(8+2m)(9+2m)(10+2m)(11+2m)}n^{2m+2} \tag{51}$$

$$C(M) = \frac{6n^2-8}{1-n^2}A(M) - 7\frac{(1-n^2)}{n^9}\left\{\frac{n^3}{3} + \frac{n^5}{5} + \frac{n^7}{7} - \frac{n^3}{1-n^2} + \frac{n}{1-n^2} + \log\sqrt{\frac{1+n}{1-n}}\right\} \tag{52}$$

$$C(M) = -\frac{2n^2}{1-n^2}A(M) + 7(1-n^2)\sum_{s=0}^{\infty}\frac{n^{2s}}{2s(8+2s)(9+2s)} \qquad (53)$$

Curves of these functions are given in Figures 2 to 11.

PART III

APPLICATION OF THE BOUNDARY LAYER EQUATIONS

A. Modifications to the Potential Nozzle Shape.

Having determined the variation of displacement thickness in the preceding sections, the next step is to obtain the modification of the potential, or perfect fluid, nozzle shape based on this thickness. The type of modification depends upon the purpose for which the nozzle is intended, or upon the type of potential design utilized.

The simplest modification is that for an axially symmetric nozzle. In this case, increasing the cross-section radius by an amount equal to the displacement thickness given by equation (24) will produce a physical nozzle whose effective shape should closely match the potential nozzle shape, and thus can be expected to produce the same flow configuration. A drawing of this configuration is given in Fig. 16, and identified as a Type I modification.

If the potential nozzle has been designed from two-dimensional considerations with a rectangular cross-section and parallel side walls, (the usual practice in supersonic wind tunnels) the question then arises as to the effect of the boundary layer in the corners. G. F. Carrier (Ref. 7) has determined the filleting effect of the boundary layer in the incompressible case, and it seems reasonable to assume that the effect will be much the same in the compressible case. Based on his results, it appears that the average radius of curvature of the displacement thickness fillet line is somewhat smaller than the thickness, and thus adds only a small amount of displacement area. In addition, another

complication arises near the corners due to the unequal boundary layer growth on the side walls and on the top. At high Mach numbers, the boundary layer on the side walls will be considerably thinner than that on the top, due to the attenuation caused by the extreme side wall height ratio. A detailed analysis of the effects which this configuration might have on the flow is extremely difficult and beyond the scope of this paper, therefore the plausible assumption will be made here that the net effect upon the displacement area due to corner interaction is negligible.

Based on this assumption, the reduction in potential flow area through the nozzle due to viscosity will be considered as equivalent to the area contained in a sharp cornered displacement thickness ring around the cross-section, as indicated in Fig. 16. With this simplification, the modification could consist of displacing each wall outward by the displacement thickness for that wall, which makes the effective shape the same as the original potential shape. The modification is essentially the same as that in the axially symmetric case, and is also called Type I.

However, this type of modification introduces a curvature into the side walls due to the non-linear rate of growth of boundary layer along the nozzle length, a factor which is undesirable in wind tunnels, both from the structural viewpoint and from considerations of flow measurement techniques. It is usual practice to incorporate windows in the tunnel side walls through which the flow configuration is observed by Schlieren or other optical means, thus any side wall curvature will introduce considerable distortion into these highly

sensitive observations. A second type of modification without this objection is that of leaving the side walls parallel and providing a sufficient area correction to the top and bottom walls which will compensate for the displacement thickness area on all four walls.

This Type II modification produces a different geometric complication due to changing the width-height ratio of the potential nozzle exit, which can be rectified by use of a suitable scale change. For example, if the design nozzle exit is square and must remain so for structural reasons, the height and length of the modified nozzle must be reduced by a suitable scale factor so as to retain a square nozzle exit or test section without distorting the two-dimensional expansion shape. Referring to Fig. 17, this problem consists of satisfying the following geometric relations,

$$y = h + \Delta h \qquad y_e = \bar{h}_e \qquad w = \bar{w} \tag{54}$$

$$\frac{\ell}{\bar{\ell}} = \frac{h}{\bar{h}} = \frac{\delta_2^*}{\bar{\delta}_2^*} = \frac{\delta_3^*}{\bar{\delta}_3^*} \equiv s \tag{55}$$

$$\bar{\delta}_2^* \, \bar{h} = (\bar{w} - \bar{\delta}_2^*)(\Delta\bar{h} - \bar{\delta}_3^*) \tag{56}$$

where Δh is the additional height of the side walls to compensate for the boundary layer on all four walls. The ratio $\Delta h/\delta_3^*$ can be found as a function of four other ratios

$\bar{a} = \dfrac{\bar{h}}{\bar{w}}$, the potential section aspect ratio, and

$\bar{b} = \dfrac{\bar{\delta}_2^*}{\bar{\delta}_3^*}$, the side-top wall displacement thickness ratio

$\bar{c} = \dfrac{\bar{\delta}_2^*}{\bar{w}}$, the displacement thickness-width ratio

$\bar{d} = \dfrac{\bar{\delta}_3^*}{\bar{h}}$, the displacement thickness-height ratio

Solving for $\Delta\bar{h}/\delta_3^*$ from equation (56)

$$\frac{\Delta\bar{h}}{\bar{\delta}_3^*} = \frac{\bar{h}\bar{b} + \bar{w} - \bar{\delta}_2^*}{\bar{w} - \bar{\delta}_2^*} = 1 + \frac{\bar{h}\bar{b}}{\bar{w} - \bar{\delta}_2^*} = 1 + \frac{\dfrac{\bar{h}}{\bar{w}}\bar{b}}{1 - \bar{c}}$$

so that

$$\frac{\Delta\bar{h}}{\bar{\delta}_3^*} = 1 + \frac{\bar{a}\bar{b}}{1 - \bar{c}} \tag{57}$$

If the potential nozzle length and height have been reduced by the scale factor s, the final ratio becomes

$$\frac{\Delta h}{\delta_3^*} = 1 + \frac{s\bar{a}\bar{b}}{1 - s\bar{c}} \tag{58}$$

The scale factor s can be obtained from the geometrical requirement that at the nozzle exit

$$y = \bar{h} = h + \Delta h = s\bar{h} + s\bar{\delta}_3^* \left(1 + \frac{s\bar{a}\bar{b}}{1 - s\bar{c}}\right) \tag{59}$$

where the exit subscript has been omitted for clarity.

$$\bar{h}(1-s\bar{c}) = s\bar{h}(1-s\bar{c}) + s\bar{\delta}_3^*(1-s\bar{c}) + s^2\bar{a}\bar{b}\bar{\delta}_3^*$$

$$s^2(\bar{a}\bar{b}\bar{\delta}_3^* - \bar{h}\bar{c} - \bar{\delta}_3^*\bar{c}) + s(\bar{h} + \bar{\delta}_3^* + \bar{h}\bar{c}) - \bar{h} = 0$$

Since $\bar{h}\bar{c} = \bar{a}\bar{b}\bar{\delta}_3^*$, this becomes

$$(\bar{\delta}_3^*\bar{c})s^2 - (\bar{h} + \bar{\delta}_3^* + \bar{h}\bar{c})s + h = 0$$

with the single physical root

$$s = \frac{(\bar{h} + \bar{\delta}_3^* + \bar{h}\bar{c}) - \sqrt{(\bar{h} + \bar{\delta}_3^* + \bar{h}\bar{c})^2 - 4\bar{h}\bar{c}\bar{\delta}_3^*}}{2\bar{c}\bar{\delta}_3^*}$$

Introducing $\bar{d} = \frac{\bar{\delta}_3^*}{\bar{h}}$, this can be written as

$$s = \frac{(1+c+d) - \sqrt{(1+c+d)^2 - 4cd}}{2cd} \qquad (60)$$

When $\bar{c}$ and $\bar{d}$ are very small, the radical can be expanded as a power series and combined with the other terms to give the simpler form

$$s = \frac{1}{1+\bar{c}+\bar{d}} \qquad (61)$$

useful for $\bar{c} < 0.1$ and $\bar{d} < 0.1$.

This scale factor is plotted in Fig. 19 as a function of the two ratios $\bar{c}$ and $\bar{d}$.

Still another type modification occurs in the case of an axially symmetric nozzle for which the nozzle exit size must remain fixed. In this Type III modification, a scale reduction factor must also be determined which will satisfy the relations at the nozzle exit that

$$\bar{y} = y + \Delta y = s(\bar{y} + \Delta\bar{y}) \equiv r \tag{62}$$

$$s = \frac{\ell}{\bar{\ell}} = \frac{r}{\bar{r}} = \frac{\delta^*}{\bar{\delta}^*} = \frac{\Delta y}{\Delta\bar{y}} \tag{63}$$

This configuration is shown in Fig. 18 and is much simpler than the Type II modification, for only one ratio enters:

$$e = \frac{\bar{\delta}^*}{\bar{y}} = \frac{\Delta\bar{y}}{\bar{y}}$$

Using this ratio and equation (62), the scale factor can be found immediately as

$$s = \frac{\bar{y}}{\bar{y} + \Delta\bar{y}} = \frac{\bar{y}}{y + \bar{\delta}^*} = \frac{1}{1 + \frac{\bar{\delta}^*}{\bar{y}}} = \frac{1}{1 + \bar{e}} \tag{64}$$

The Type III scale factor agrees formally with that in the Type II modification for the limiting case where either $\bar{c}$ or $\bar{d}$ vanishes and thus may be conveniently obtained from Fig. 19 by considering $\bar{c} = 0$ and $\bar{e} = \bar{d}$.

In the determination of the shrinkage factors for Type II and III modifications, the effect which the reduction in Reynolds number has upon the wall friction coefficient and thus the boundary layer thickness is of

second order magnitude; subsequently it has been neglected in the analysis.

B. Application to a Specific Nozzle.

As an illustration of the procedure, the methods developed in the previous sections are applied to the design of a two-dimensional wind tunnel nozzle having a square exit and a design Mach number near ten. The major steps in this application consist of:

1) Obtaining the initial potential nozzle shape.

2) Determining the boundary layer growth on the top and side walls of the potential nozzle.

3) Computing the modification to the potential shape to compensate for the boundary layer growth.

The initial potential nozzle shape can best be obtained by analytical means (Refs. 2, 3, 4) for the graphical method is subject to considerable error due to the small Mach angles corresponding to the high Mach numbers in the major portion of the nozzle. The procedure utilized here is Puckett's modification of Foelsch's method (Ref. 3). The general potential nozzle configuration is shown in Fig. 20, where the wall ordinates ξ, h are given by the equations:

$$\frac{\xi}{h_e} = \frac{\cos(\nu_e - \nu)}{\theta_m} \frac{t}{t_e} \left\{ 1 + (\nu - \nu_m) \left[\sqrt{M^2 - 1} - \tan(\nu_e - \nu) \right] \right\} \qquad (65)$$

$$\frac{h}{h_e} = \frac{\sin(\nu_e - \nu)}{\theta_m} \frac{t}{t_e} \left\{ 1 + (\nu - \nu_m) \left[\sqrt{M^2 - 1} + \cot(\nu_e - \nu) \right] \right\} \qquad (66)$$

where

$$\frac{t}{te} = \frac{\text{section area}}{\text{exit area}} = \frac{S/S^*}{Se/S^*} = \frac{t}{te} \quad (M)$$

ψ = Prandtl-Meyer angle

θ_m = maximum wall expansion angle.

The radius of curvature of the arc forming the wall shape from the throat to the maximum expansion point is obtained from

$$R_t = \frac{h_m - h^*}{1 - \cos\theta_m} = \frac{h_e}{1 - \cos\theta_m}\left\{\frac{\sin\theta_m}{\theta_m}\frac{t_m}{te} - \frac{t^*}{t_e}\right\} \tag{67}$$

since

$$\frac{h^*}{h_e} = \frac{t^*}{te} \qquad \frac{h_m}{h_e} = \frac{\sin\theta_m}{\theta_m}\frac{t_m}{te} \tag{68}$$

The distance from the throat to the theoretical point source is given by

$$x_s = R_t \sin\theta_m - \xi_m = h_e\left\{\frac{1}{\theta_m}\frac{t_m}{te} - \frac{\sin\theta_m}{1-\cos\theta_m}\frac{t^*}{te}\right\} \tag{69}$$

while the distance from the source to the maximum expansion point is found from

$$\frac{\xi_m}{h_e} = \frac{\cos\theta_m}{\theta_m}\frac{t_m}{te} \tag{70}$$

The distance from point source to nozzle exit is obtained from

$$\frac{\xi_e}{h_e} = \frac{1}{\theta_m} + \sqrt{M^2 - 1} \tag{71}$$

so that the total nozzle length is given by

$$\frac{x_e}{h} = \frac{\ell}{h} = \frac{1}{\theta_m}\left(1 + \frac{t_m}{t_e}\right) - \frac{\sin\theta_m}{1-\cos\theta_m}\left(\frac{t^*}{t_e}\right) + \sqrt{M^2-1} \qquad (72)$$

The choice of the three design parameters ψ_e, $\bar{h}_e$ and θ_m uniquely determines the initial potential nozzle size and shape; for this example, their values have been taken as

$$\psi_e = 102^\circ \quad \text{(corresponding to M = 9.98)}$$

$$\bar{h}_e = 10"$$

$$\theta_m = 30^\circ$$

With these values, the initial nozzle length and throat half-height are found to be, respectively,

$$\bar{\ell} = 117.40" \quad \text{and} \quad \bar{h}^* = 0.01974"$$

The other wall ordinates for the initial nozzle are tabulated in the first half of Fig. 21.

The next design step is that of determining the boundary layer growth along this initial potential nozzle. The rate of growth as determined by this method is a function only of two parameters, the wall friction coefficient, and the choice of velocity profile. Each of these in turn depends somewhat upon the Reynolds number of the flow, which can be expressed in terms of the wind tunnel supply pressure and temperature. Choosing 1000 psi and 100° F as typical supply values, the Reynolds number

based on the throat height is 970,000; while that at the nozzle exit, based on the exit height, is 8,600,000. These Reynolds numbers are so high that fully developed turbulent boundary layers can be expected along the entire nozzle length. Consequently, the turbulent velocity profile will be utilized here, and the average wall friction coefficient will be taken as 0.002.

The growth of boundary layer displacement thickness along the side walls of the initial potential nozzle can now be obtained by a graphical or numerical integration of

$$\delta_2^* = \frac{1}{2} C_f \frac{h^*}{h} \frac{B(M)}{G(M)} \int_0^x \frac{h}{h^*} \frac{G(M)}{A(M)} dx \qquad (23)$$

while the displacement thickness on the top and bottom walls is found from

$$\delta_3^* = \frac{1}{2} C_f \frac{B(M)}{G(M)} \int_0^x \frac{G(M)}{A(M)} dx \qquad (23a)$$

since h/h* has the value unity for the latter walls. To reduce the amount of computation necessary for the integration of equations (23) and (23a), curves of the quantities

$$\frac{G(M)}{A(M)} \quad , \quad \frac{B(M)}{G(M)} \quad , \quad \frac{h}{h^*} \frac{G(M)}{A(M)} \quad , \quad \frac{h^*}{h} \frac{B(M)}{G(M)}$$

are plotted in Figs. 8 - 15 as functions of free stream Mach number. To enable the functions $\frac{h}{h^*} \frac{G(M)}{A(M)}$ and $\frac{h^*}{h} \frac{B(M)}{G(M)}$ to be presented as a single curve valid for all nozzles, the value of h/h* was taken as equal to the area ratio, S/S*, for the particular Mach number, as given by

$$\frac{S}{S^*} = M\left\{\frac{\frac{\gamma+1}{2}}{1+\frac{\gamma-1}{2}M^2}\right\}^{\frac{\gamma+1}{2(\gamma-1)}} = \frac{1.728\,M}{(1+0.2M^2)^3} \qquad (73)$$

The results of these integrations are shown in Fig. 21; in particular, the displacement thicknesses at the nozzle exit are found to be

$$\overline{\delta}^*_{2e} = 3.87" \quad \text{and} \quad \overline{\delta}^*_{3e} = 8.13" .$$

For this example, the boundary layer thickness on the side wall at the nozzle exit is less than half the thickness on the top wall, due to the extreme side wall height ratio.

Having the boundary layer growth along the initial potential nozzle, the final design step is to compute the modification to the potential shape. Since the nozzle exit should remain twenty inches square, a Type II modification is called for. The values of the displacement thickness width ratio and displacement thickness-height ratio turn out to be

$$\bar{c}_e = \frac{\overline{\delta}^*_{2e}}{\overline{w}_e} = \frac{3.87}{10} = 0.387$$

and

$$\bar{d}_e = \frac{\overline{\delta}^*_{3e}}{\overline{h}_e} = \frac{8.13}{10} = 0.813$$

so that the nozzle scale reduction factor can be found from Fig. 19 and has the value 0.488. The final nozzle length is

$$\ell = s\bar{\ell} = (0.488)(117.40") = 57.6" .$$

Next, the wall corrections, Δh, are obtained from

$$\frac{\Delta h}{\delta^*_3} = 1 + \frac{s\bar{a}\bar{b}}{1 - s\bar{c}} \qquad (58)$$

and added to the reduced potential nozzle ordinates to give the final nozzle ordinates, where

$$y_i = h_i + \Delta h_i = s\bar{h}_i + s\Delta\bar{h}_i \qquad (54)$$

The resulting nozzle ordinates are given in Fig. 21, and the final nozzle shape is drawn to scale in Fig. 22. Note that the boundary layer correction amounts to slightly over 50% of the nozzle exit area for this configuration; or, conversely, the potential flow core consists of only 48.8% of the total exit area.

REFERENCES

1. Puckett, A. E., "Supersonic Nozzle Design", Journal of Applied Mechanics, December, 1946.

2. Atkin, A. O. L., "Two-Dimensional Supersonic Channel Design", R and M No. 2174, November, 1945.

3. Foelsch, Kuno, "A New Method of Designing Two-Dimensional Laval Nozzles for a Parallel and Uniform Jet", North American Report NA-46-235, March, 1946.

4. Foelsch, Kuno, "The Analytical Design of an Axially Symmetric Laval Nozzle for a Parallel and Uniform Jet", Journal of the Aeronautical Sciences, March, 1949.

5. Durand, W. F., "Aerodynamic Theory, Vol. III", Durand Reprinting Committee, California Institute of Technology, January, 1943, p. 102 et seq.

6. Lewis, J. A., "Monograph V, Boundary Layer in Compressible Fluid", Tech Report No. F-TR-1179-ND, Air Materiel Command, February, 1948.

7. Carrier, G. F., "The Boundary Layer in a Corner", Quarterly of Applied Mathematics, January, 1947, p. 367.

NOTATION

a	speed of sound
$\bar{a} = \frac{\bar{h}}{\bar{w}}$	cross-section aspect ratio
$\bar{b} = \bar{\delta}_2^* / \bar{\delta}_3^*$	side-top wall displacement thickness ratio
$c = \sqrt{\frac{\gamma+1}{\gamma-1}}\, a^*$	maximum velocity obtainable by isentropic expansion into a vacuum
$\bar{c} = \frac{\bar{\delta}_2^*}{\bar{w}}$	displacement thickness-width ratio
$\bar{d} = \frac{\bar{\delta}_3^*}{\bar{h}}$	displacement thickness-height ratio
$e = 2.718\ldots$	base of natural logarithms
$\bar{e} = \frac{\bar{\delta}^*}{\bar{g}}$	displacement thickness-radius ratio
g	potential nozzle station radius
h	potential nozzle station half-height
ℓ	nozzle length
$n = \frac{u_1}{c}$	normalized fluid velocity
p	static pressure
r	physical nozzle station radius
s	nozzle scale reduction factor
$t = \frac{S}{S^*}$	area ratio
u	velocity parallel to wall and nozzle axis
v	velocity normal to wall

w	potential nozzle station half-width
x	nozzle length ordinate
x_s	distance from throat to point source
y	physical nozzle station half-height
z	physical nozzle station half-width
$A = \frac{\vartheta}{\delta}$	dimensionless momentum thickness
$B = \frac{\delta^*}{\delta}$	dimensionless displacement thickness
$C = u_1 \frac{dA}{du_1}$	
$C_f = \frac{\tau_o}{\frac{1}{2}\rho_1 u_1^2}$	wall friction coefficient
$D = (2 - M_1)A + B + C$	
$G = e^{\int \frac{D}{A} \frac{du_1}{u_1}}$	
$H = e^{\int \frac{dh}{h}} = \frac{h}{h^*}$	
M	Mach number
R	Reynolds number
R_t	throat radius of curvature
S	cross-sectional area
T	temperature
$\gamma = 1.400$	ratio of specific heats

δ	total boundary layer thickness
δ_t	throat boundary layer thickness
δ^*	boundary layer displacement thickness
δ_2^*	side wall displacement thickness
δ_3^*	top wall displacement thickness
η	dimensionless ordinate normal to wall
ϑ	boundary layer momentum thickness
θ	wall expansion angle
ξ	distance from source along x axis
ρ	fluid density
σ	Prandtl number
τ_o	shearing stress at the wall
ψ	Prandtl-Meyer angle
ω	dimensional velocity within the boundary layer

Subscripts

$( )_o$	stagnation conditions in the flow
$( )_1$	flow conditions outside the boundary layer, i.e. free stream conditions
$( )_e$	conditions at the nozzle exit

$(\ )_i$	dimension at station "i"
$(\ )_m$	conditions at maximum wall expansion angle
no subscript	conditions within the boundary layer; or final nozzle dimension

Superscripts

$(\ )^*$	conditions at $M_1 = 1$ (except for δ^*)
$(\overline{\ })$	initial nozzle dimension

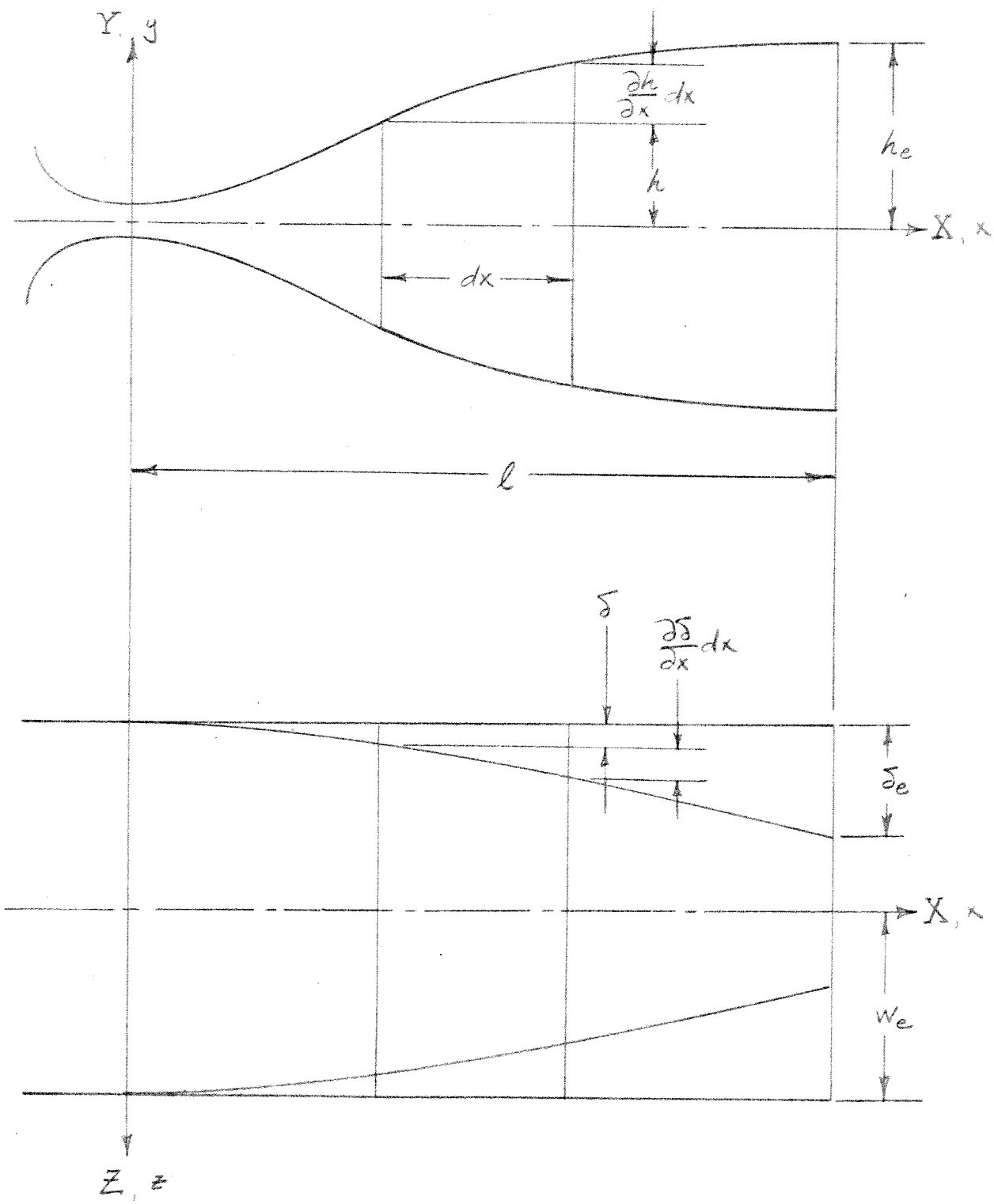

BOUNDARY LAYER SEGMENT

FIG 1

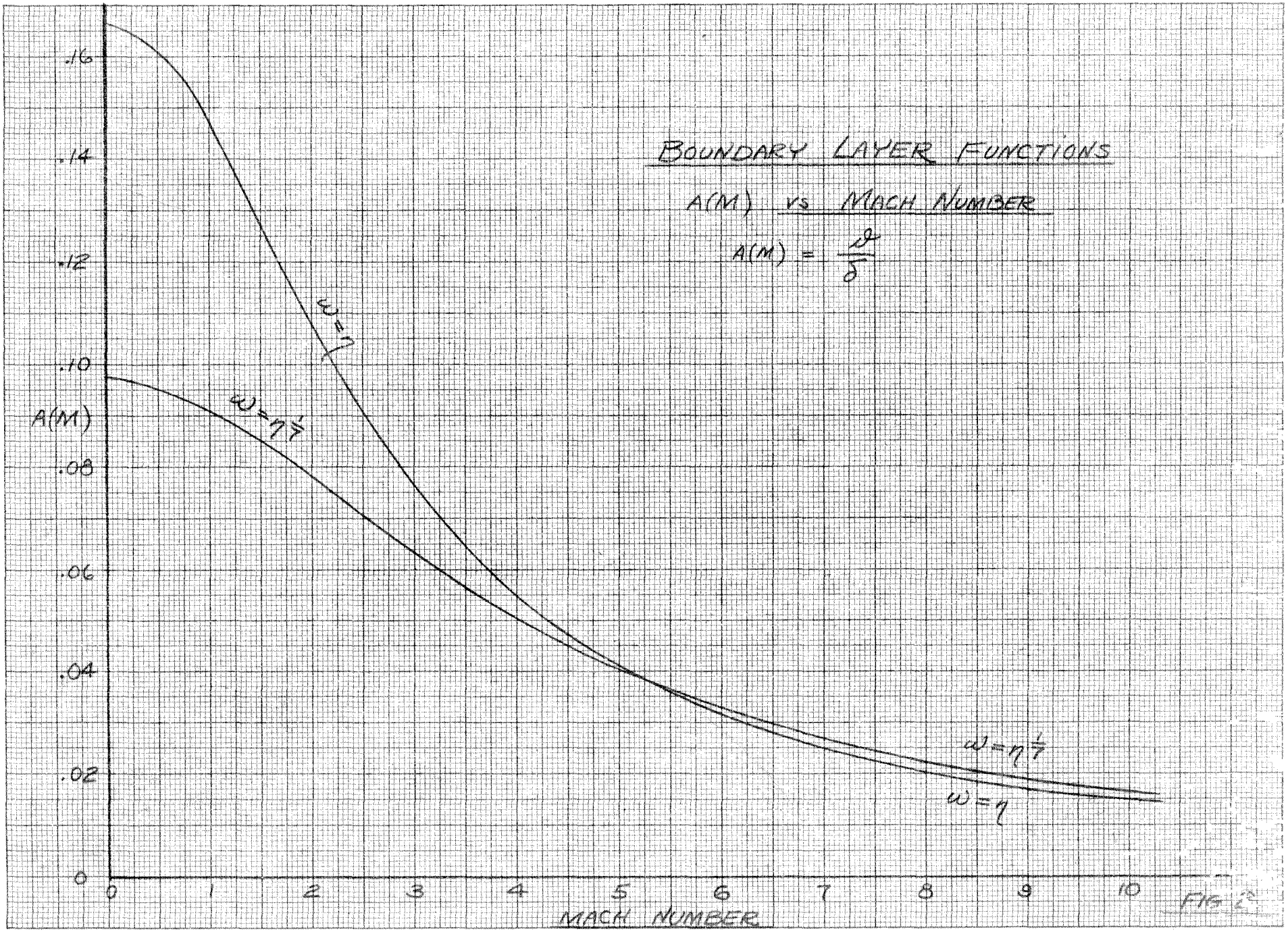
BOUNDARY LAYER FUNCTIONS
A(M) vs MACH NUMBER
$A(M) = \frac{\vartheta}{\delta}$
A(M)
.16
.14
.12
.10
.08
.06
.04
.02
0
0
1
2
3
4
5
6
7
8
9
10
MACH NUMBER
$\omega = \eta$
$\omega = \eta^{\frac{1}{2}}$
$\omega = \eta^{\frac{1}{7}}$
$\omega = \eta$

FIG 2

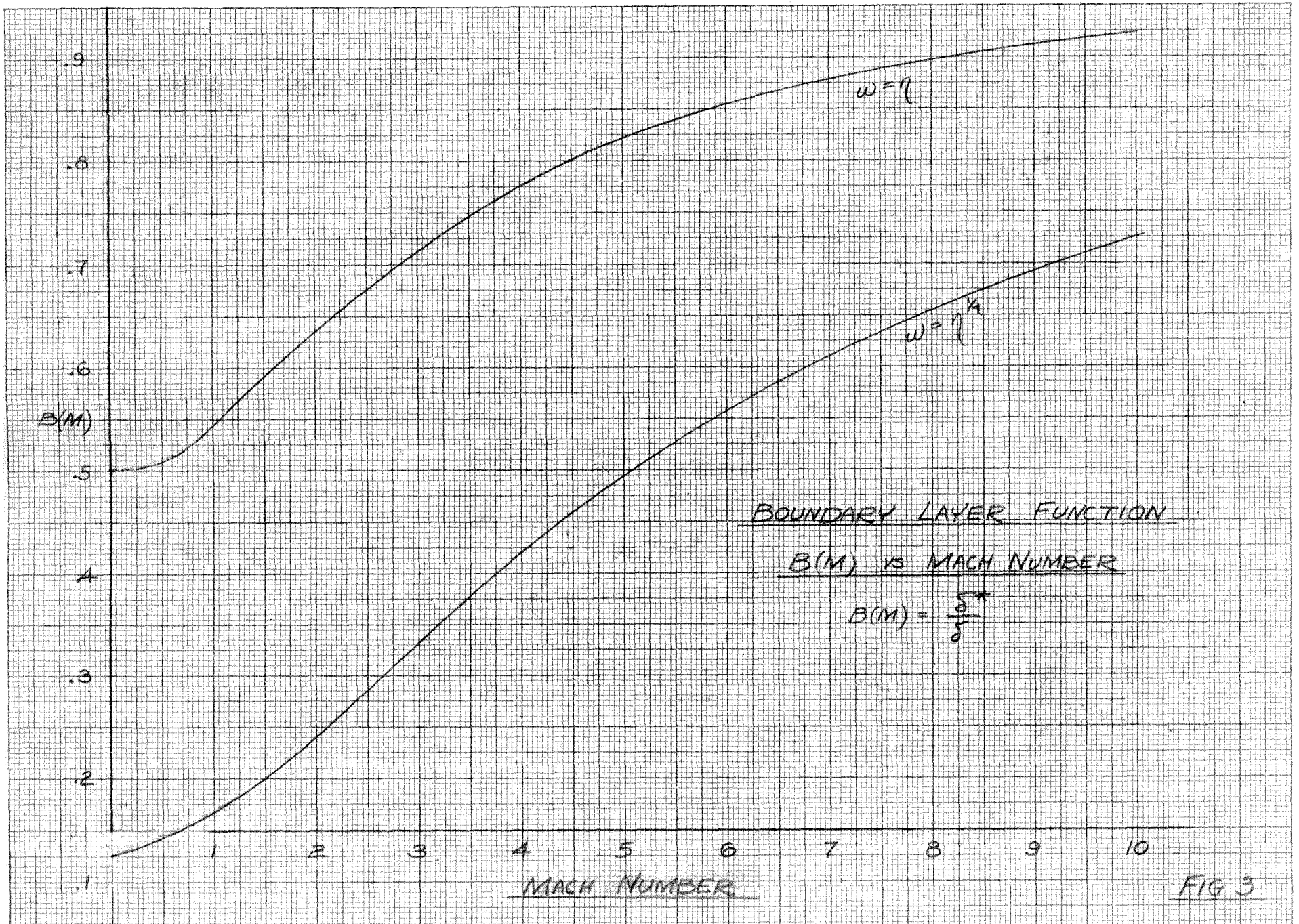
.9
.8
.7
.6
B(M)
.5
.4
.3
.2
.1
1
2
3
4
5
6
7
8
9
10
MACH NUMBER
ω = η
ω = η^1/4
BOUNDARY LAYER FUNCTION
B(M) VS MACH NUMBER
B(M) = δ*/δ

FIG 3

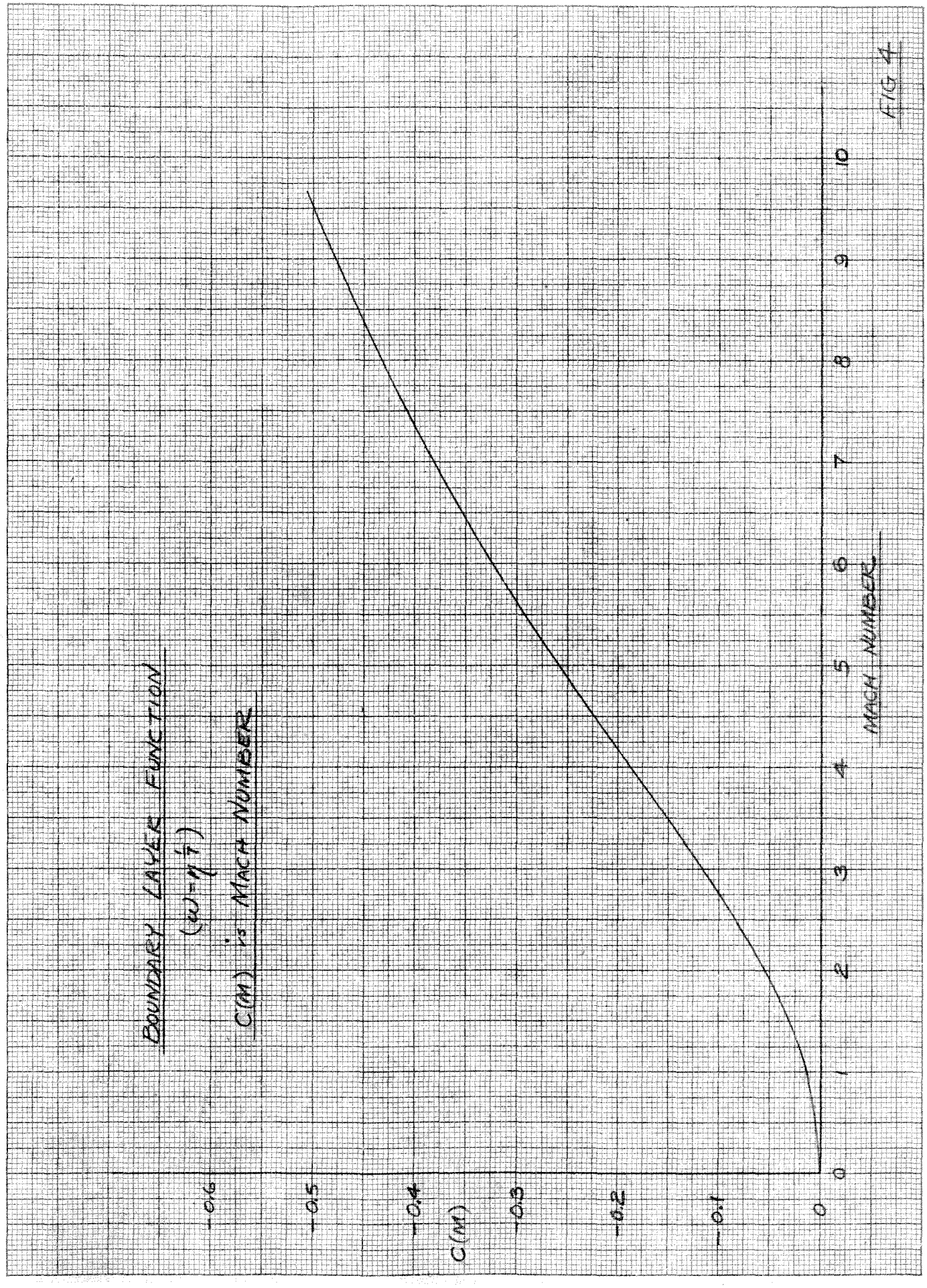
BOUNDARY LAYER FUNCTION
(ω-η f')
C(M) vs MACH NUMBER
C(M)
-0.6
-0.5
-0.4
-0.3
-0.2
-0.1
0
0
1
2
3
4
5
6
7
8
9
10
MACH NUMBER

FIG 4

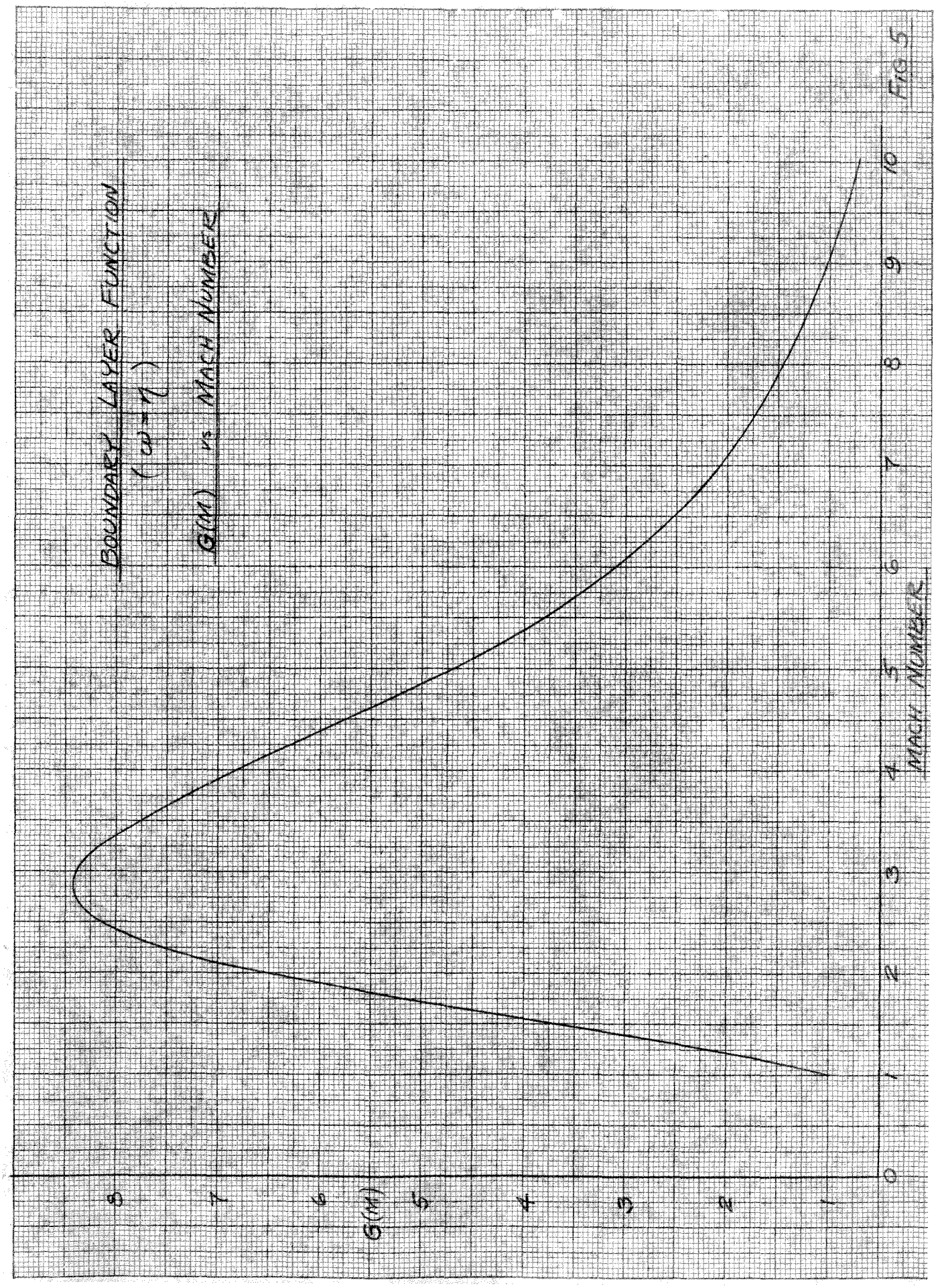
BOUNDARY LAYER FUNCTION
(ω = 1)
G(M) vs MACH NUMBER
G(M)
MACH NUMBER
0
1
2
3
4
5
6
7
8
9
10

FIG 5

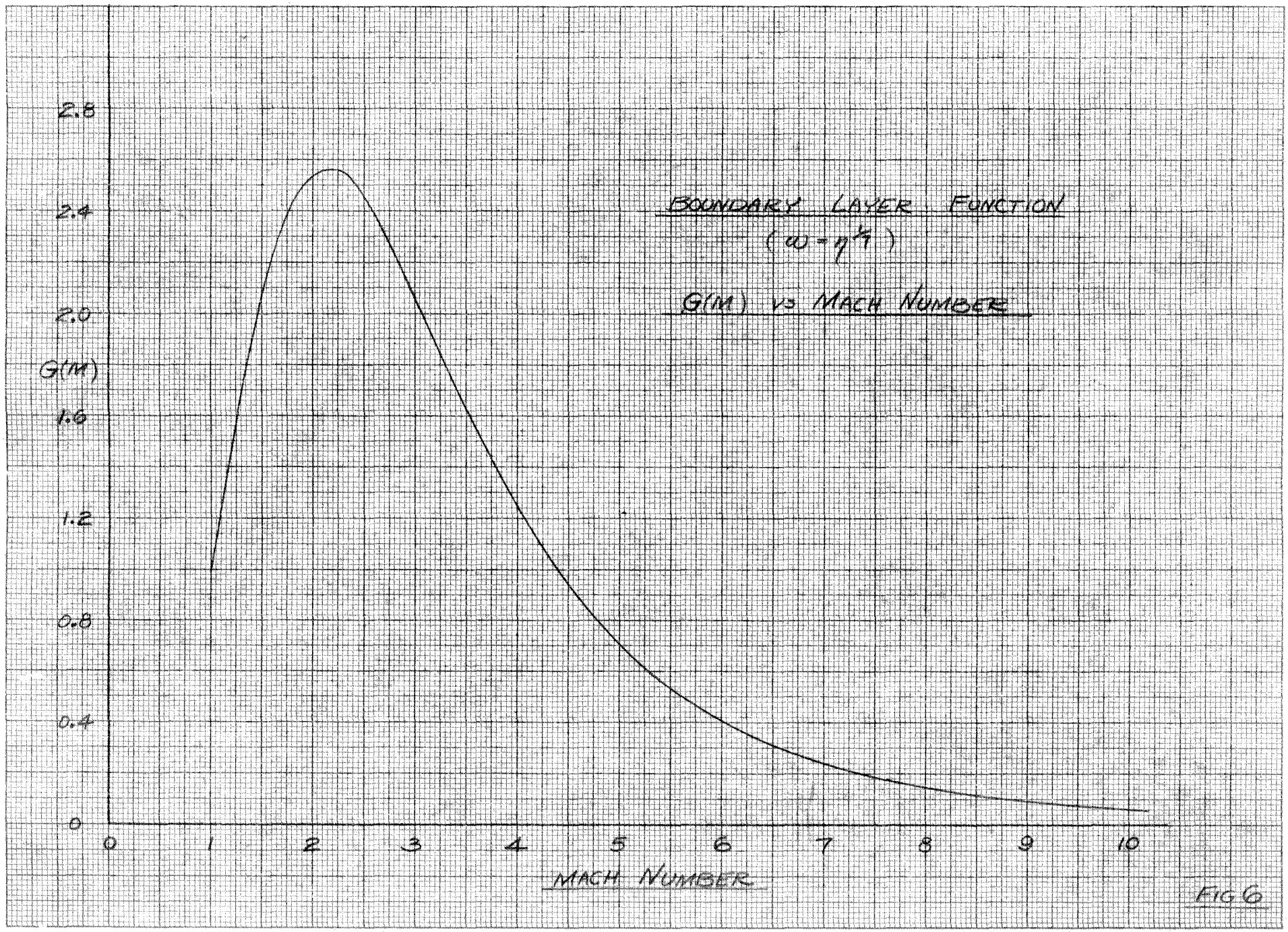
BOUNDARY LAYER FUNCTION
$(\omega = \eta^{1/4})$
G(M) vs MACH NUMBER
G(M)
2.8
2.4
2.0
1.6
1.2
0.8
0.4
0
0
1
2
3
4
5
6
7
8
9
10
MACH NUMBER

FIG 6

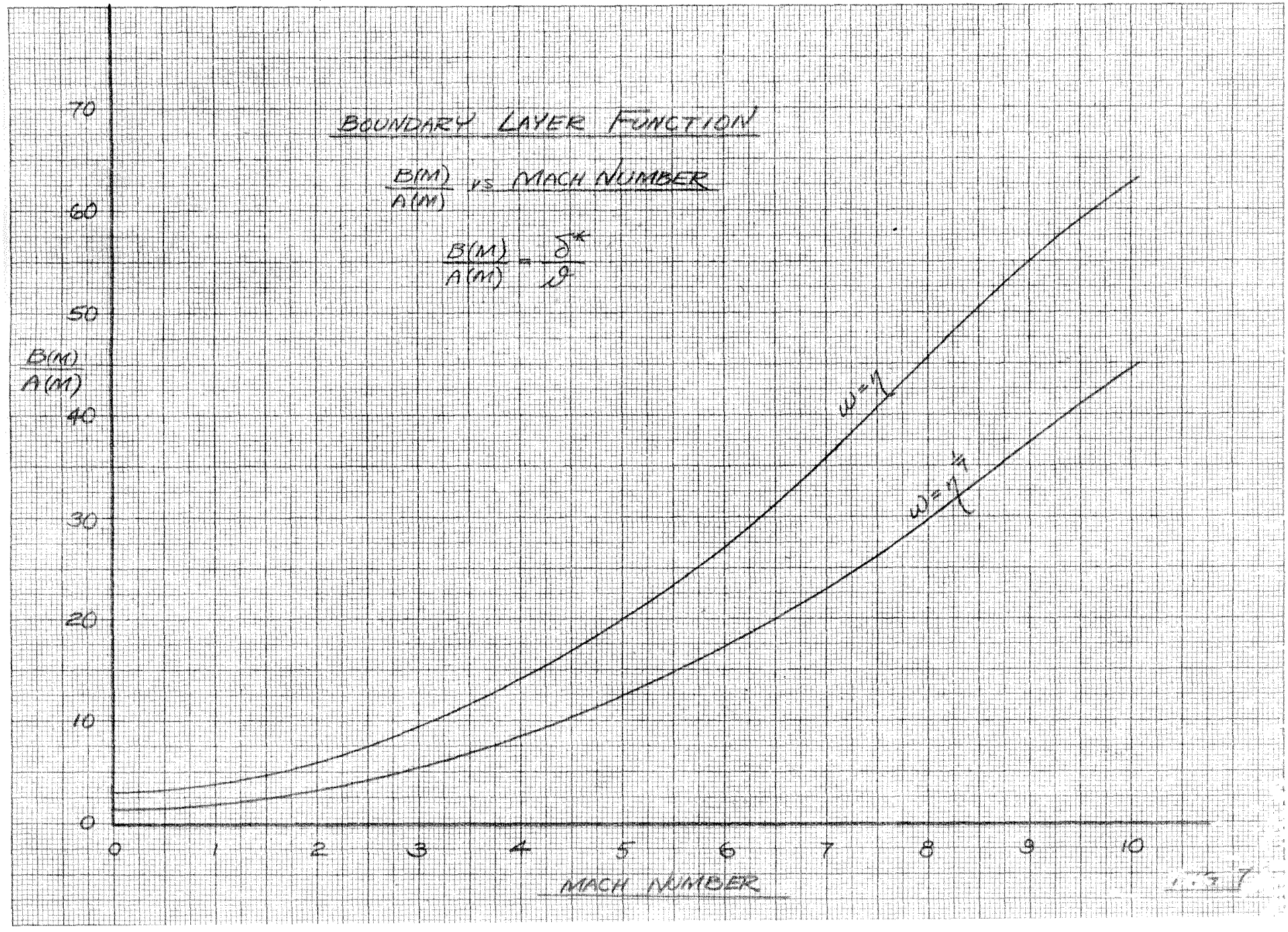
BOUNDARY LAYER FUNCTION
B(M)/A(M) vs MACH NUMBER
B(M)/A(M) = δ*/ϑ
B(M)/A(M)
70
60
50
40
30
20
10
0
0
1
2
3
4
5
6
7
8
9
10
MACH NUMBER
ω=1
ω=1/4

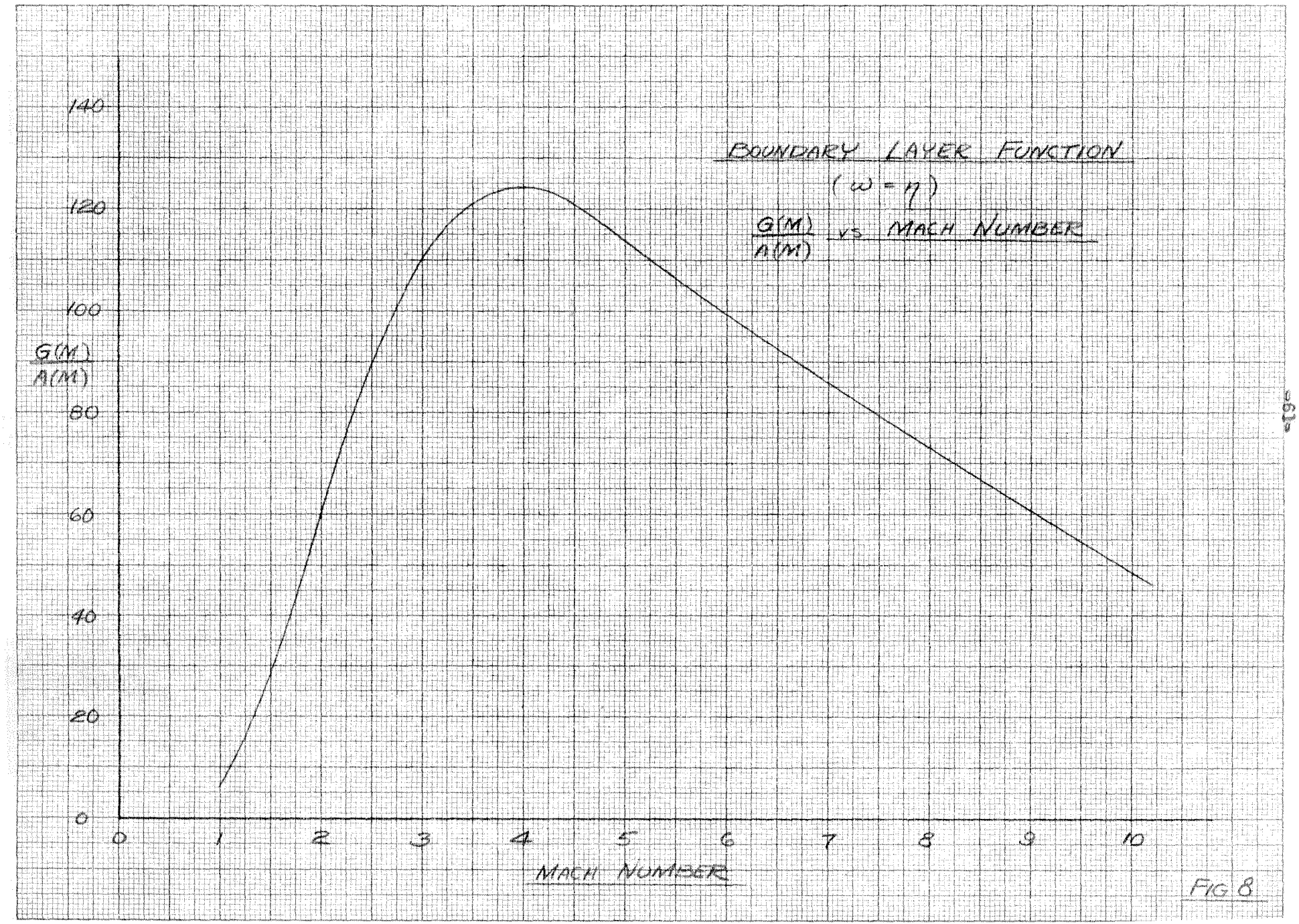
BOUNDARY LAYER FUNCTION
(ω = 7)
G(M)/A(M) vs MACH NUMBER
G(M)/A(M)
140
120
100
80
60
40
20
0
0
1
2
3
4
5
6
7
8
9
10
MACH NUMBER

FIG 8

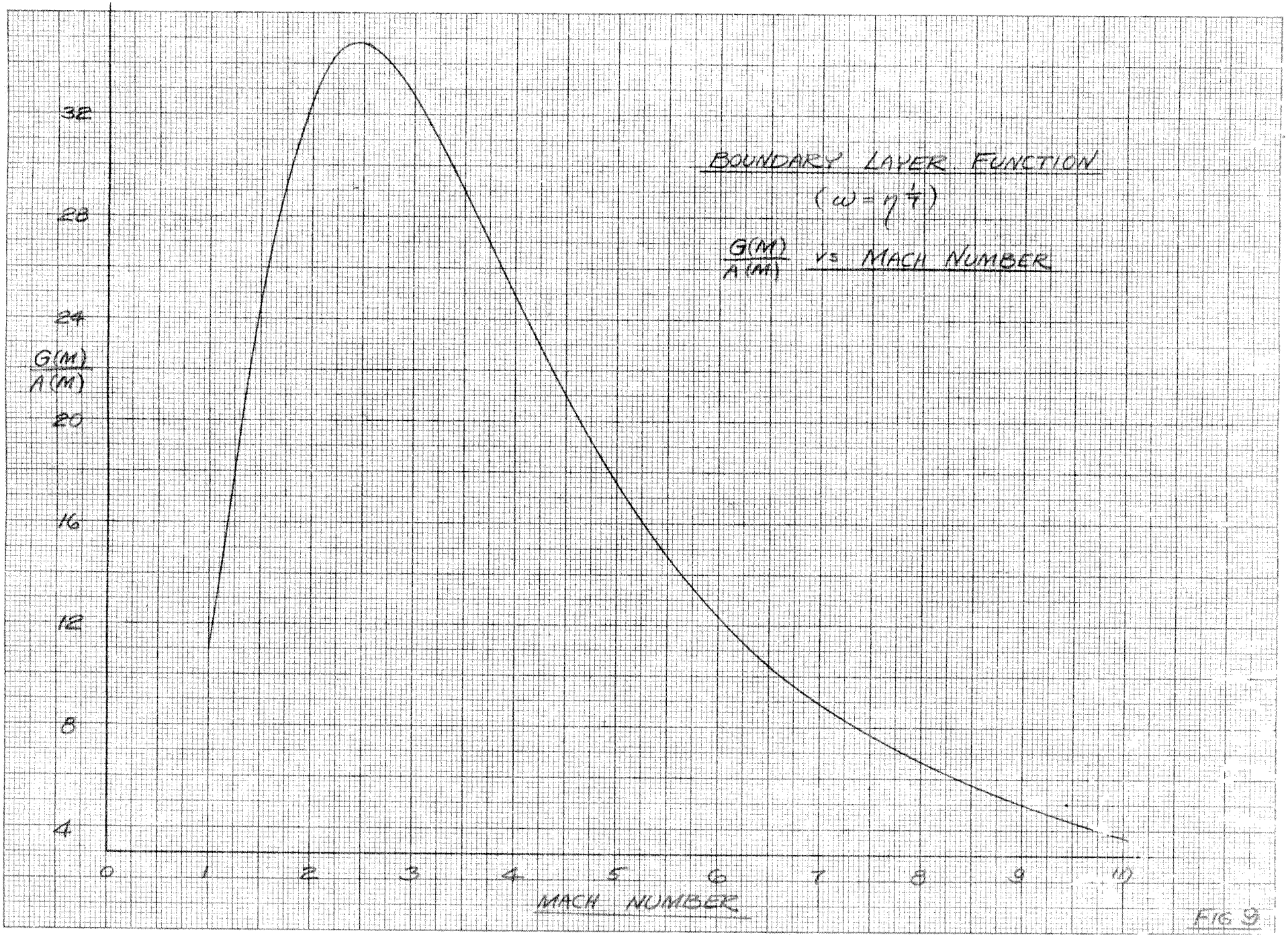
BOUNDARY LAYER FUNCTION
$(\omega = \gamma^{\frac{1}{7}})$
$\frac{G(M)}{A(M)}$ vs MACH NUMBER
$\frac{G(M)}{A(M)}$
32
28
24
20
16
12
8
4
0
1
2
3
4
5
6
7
8
9
10
MACH NUMBER

FIG 9

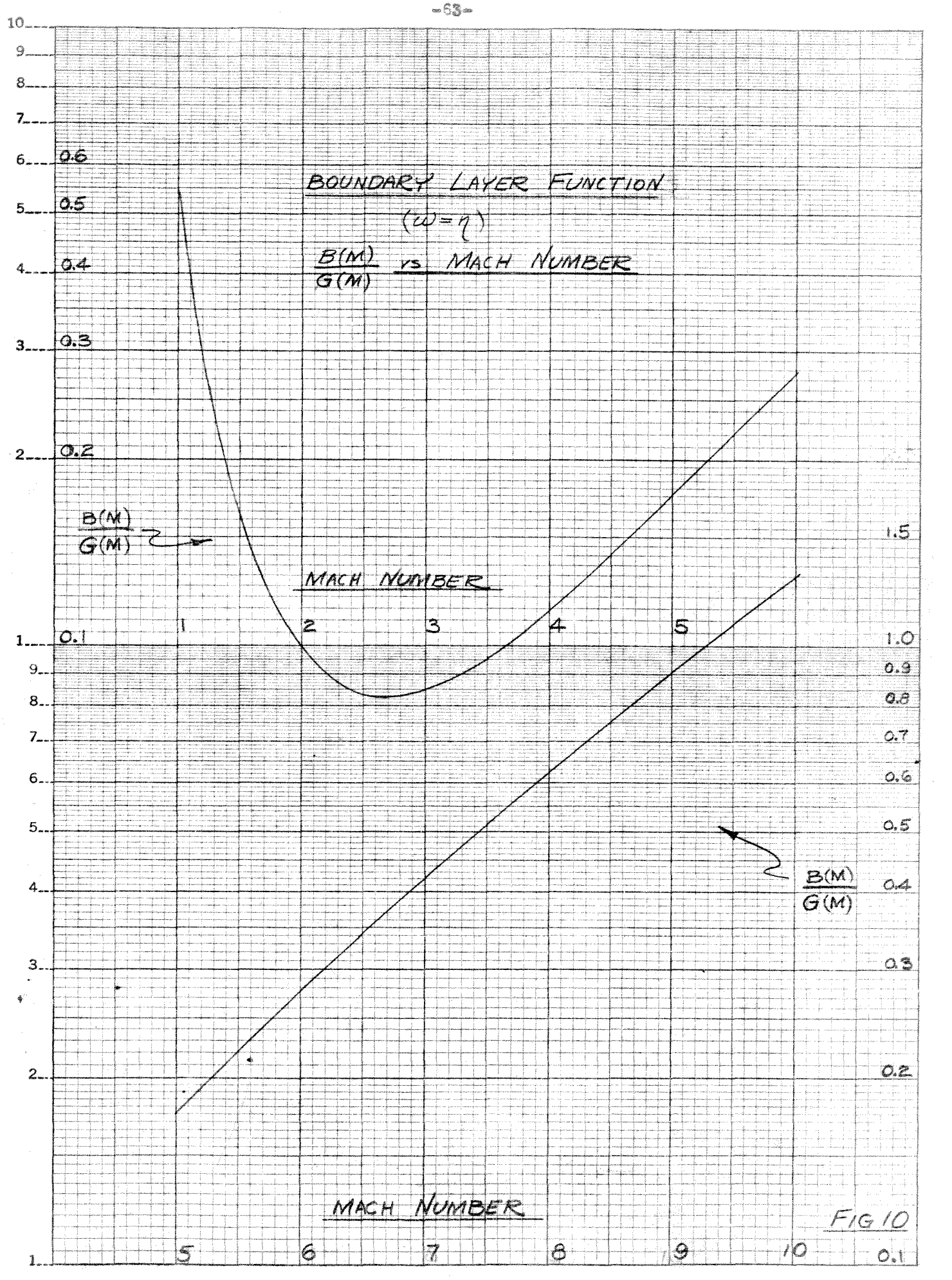
BOUNDARY LAYER FUNCTION
(ω = η)
B(M)/G(M) vs MACH NUMBER
B(M)/G(M)
MACH NUMBER
MACH NUMBER
B(M)/G(M)
0.1
0.2
0.3
0.4
0.5
0.6
1.0
1.5
1
2
3
4
5
6
7
8
9
10

FIG 10

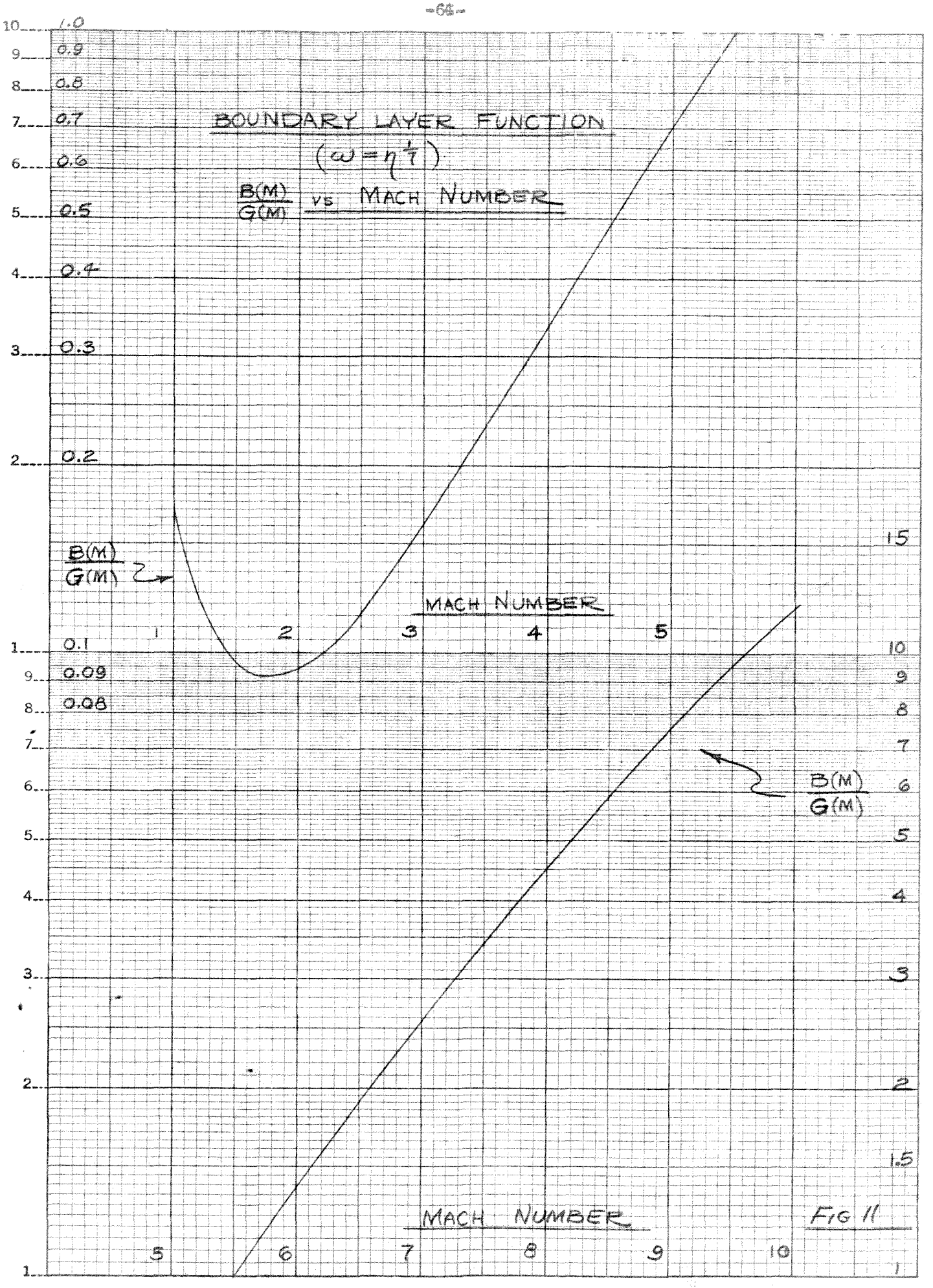
BOUNDARY LAYER FUNCTION
$(\omega = \eta^{\frac{1}{\gamma}})$
$\frac{B(M)}{G(M)}$ VS MACH NUMBER
$\frac{B(M)}{G(M)}$
MACH NUMBER
$\frac{B(M)}{G(M)}$
MACH NUMBER

FIG 11

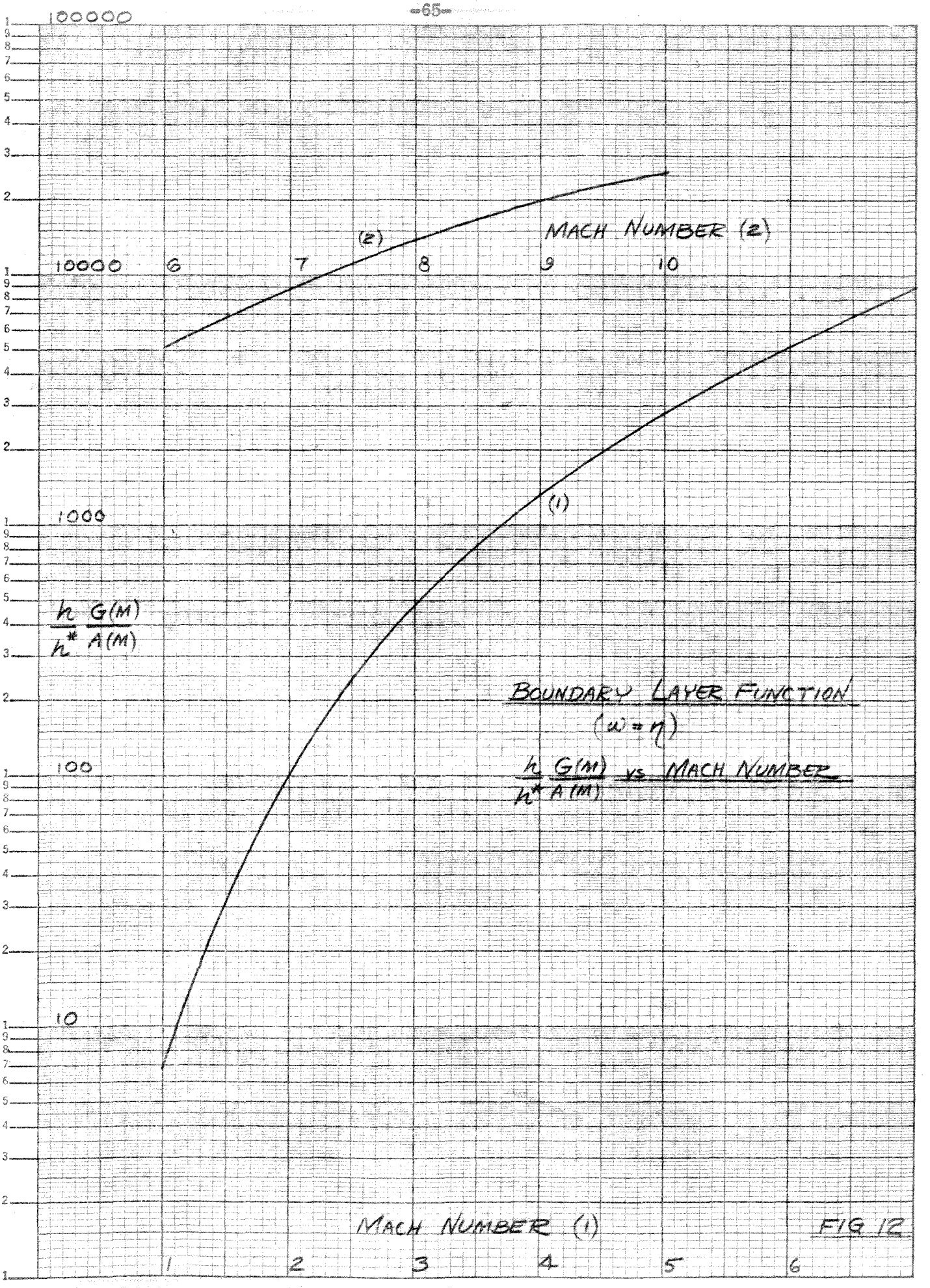
100000
10000
1000
100
10
$\frac{h}{h^*}\frac{G(M)}{A(M)}$
6
7
8
9
10
(2)
MACH NUMBER (2)
(1)
BOUNDARY LAYER FUNCTION
$(\omega = \eta)$
$\frac{h}{h^*}\frac{G(M)}{A(M)}$ vs MACH NUMBER
1
2
3
4
5
6
MACH NUMBER (1)

FIG 12

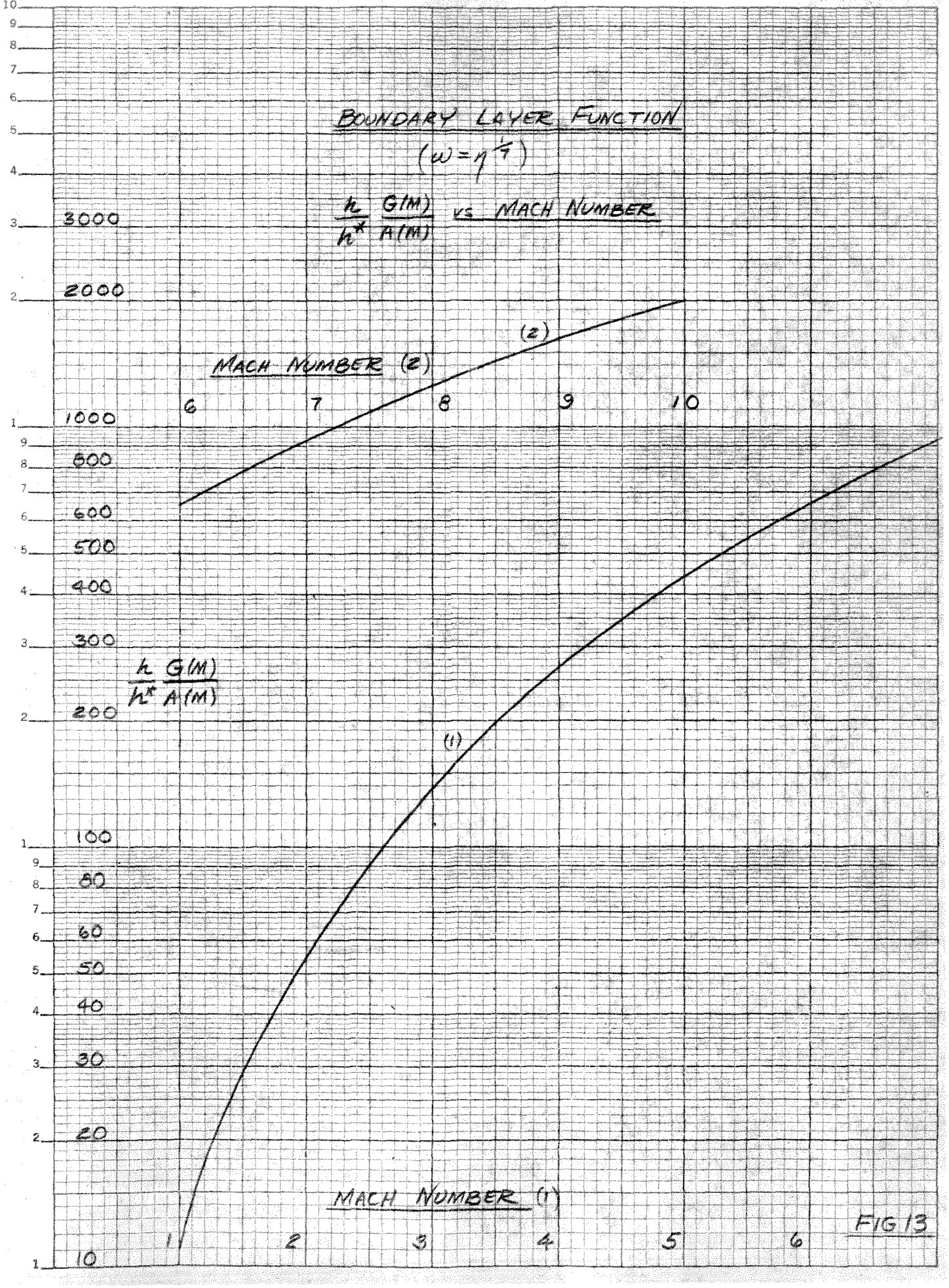
BOUNDARY LAYER FUNCTION
$(\omega = \eta^{\frac{1}{4}})$
$\frac{h}{h^*}\frac{G(M)}{A(M)}$ vs MACH NUMBER
3000
2000
1000
800
600
500
400
300
200
100
80
60
50
40
30
20
10
(2)
MACH NUMBER (2)
6
7
8
9
10
$\frac{h}{h^*}\frac{G(M)}{A(M)}$
(1)
MACH NUMBER (1)
1
2
3
4
5
6

FIG 13

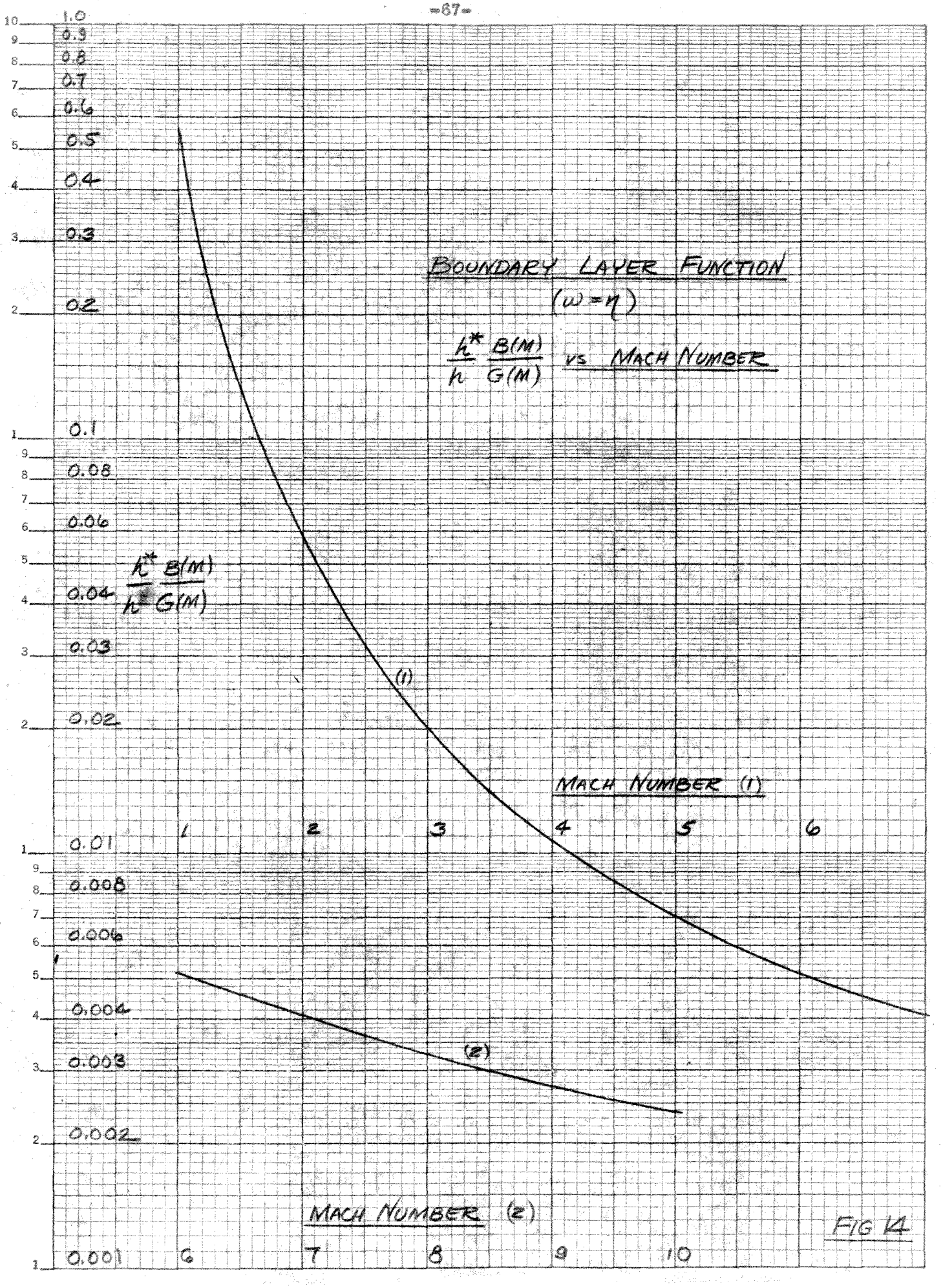
BOUNDARY LAYER FUNCTION
(ω = η)
$\frac{k^*}{h}\frac{B(M)}{G(M)}$ vs MACH NUMBER
$\frac{k^*}{h}\frac{B(M)}{G(M)}$
1.0
0.9
0.8
0.7
0.6
0.5
0.4
0.3
0.2
0.1
0.08
0.06
0.04
0.03
0.02
0.01
0.008
0.006
0.004
0.003
0.002
0.001
(1)
(2)
MACH NUMBER (1)
MACH NUMBER (2)
1
2
3
4
5
6
7
8
9
10

FIG 4

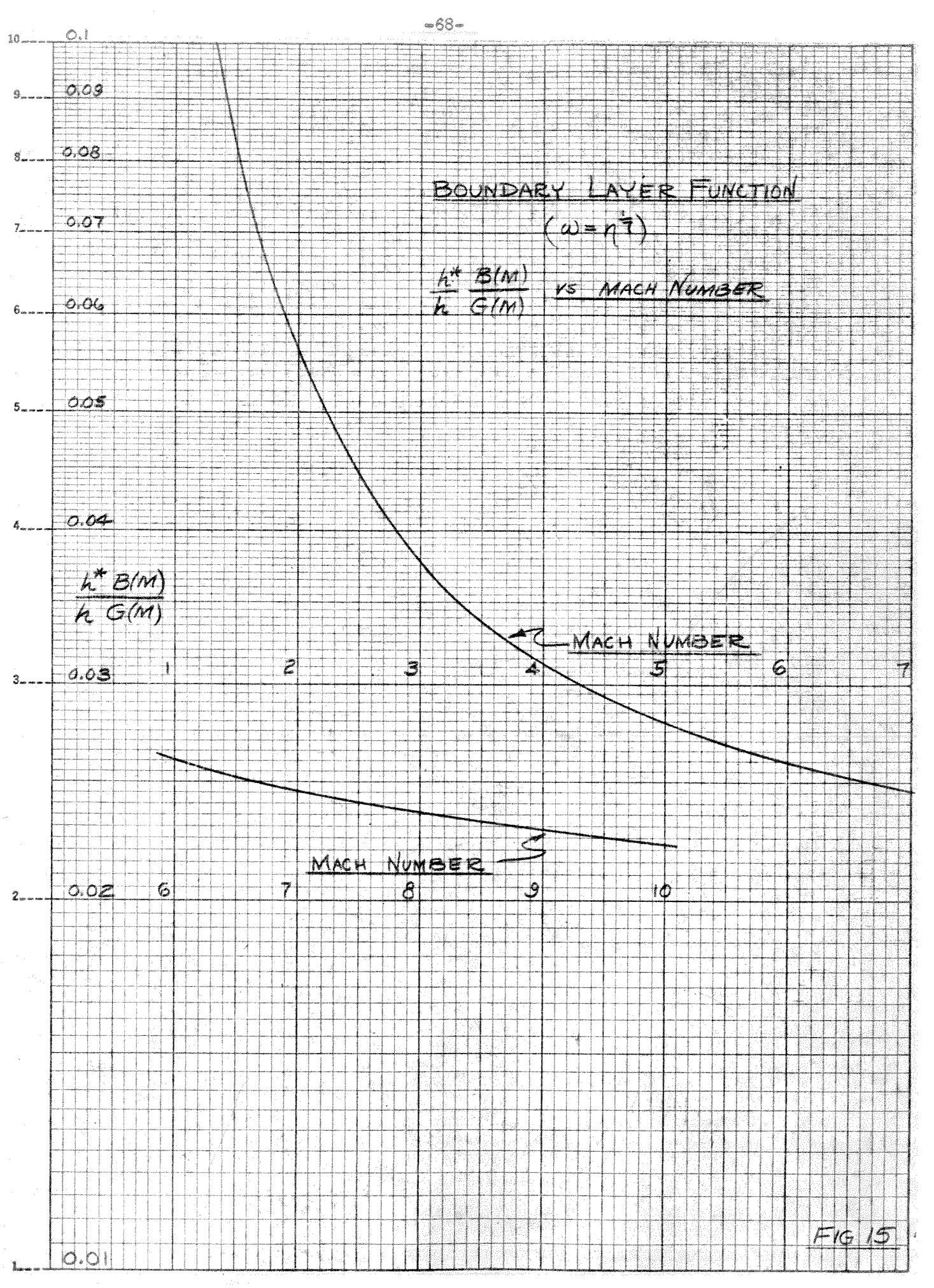
BOUNDARY LAYER FUNCTION
$(\omega = \eta^{\frac{1}{7}})$
$\frac{h^*}{h}\frac{B(M)}{G(M)}$ VS MACH NUMBER
$\frac{h^* B(M)}{h G(M)}$
MACH NUMBER
MACH NUMBER
0.1
0.09
0.08
0.07
0.06
0.05
0.04
0.03
0.02
0.01
1
2
3
4
5
6
7
8
9
10

FIG 15

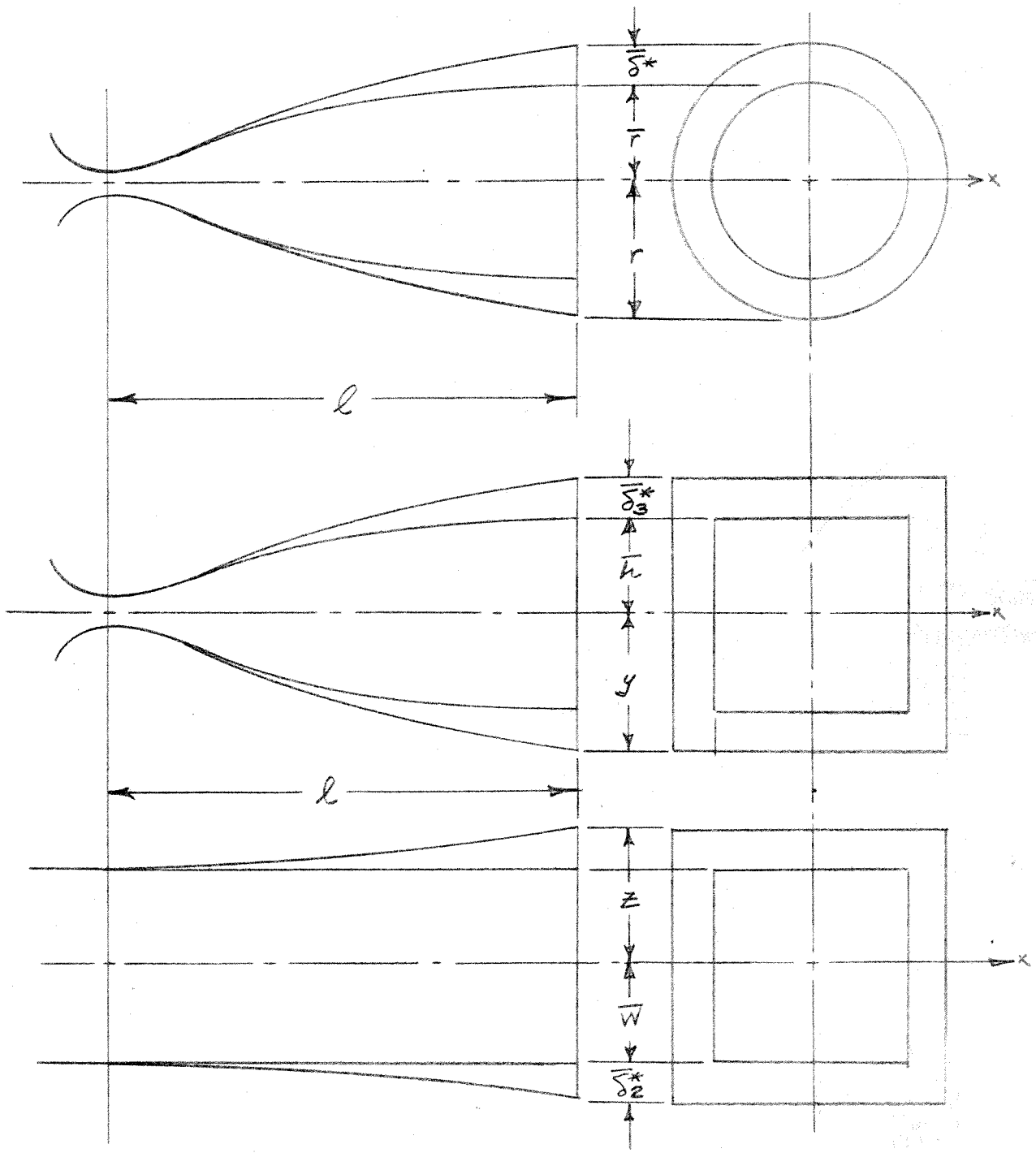

TYPE I MODIFICATION TO POTENTIAL SHAPE

FIG 16

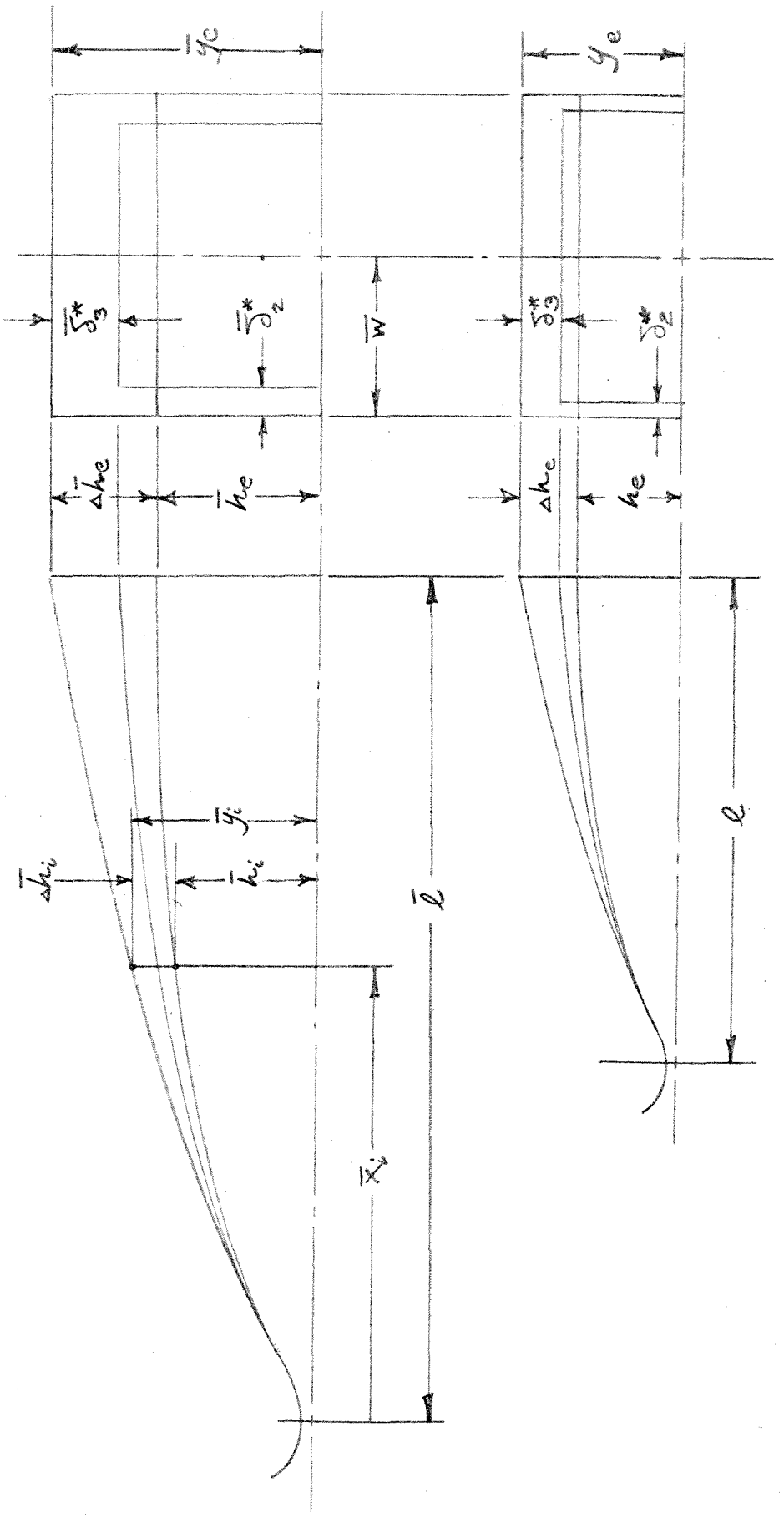

TYPE II MODIFICATION TO POTENTIAL SHAPE

FIG 17

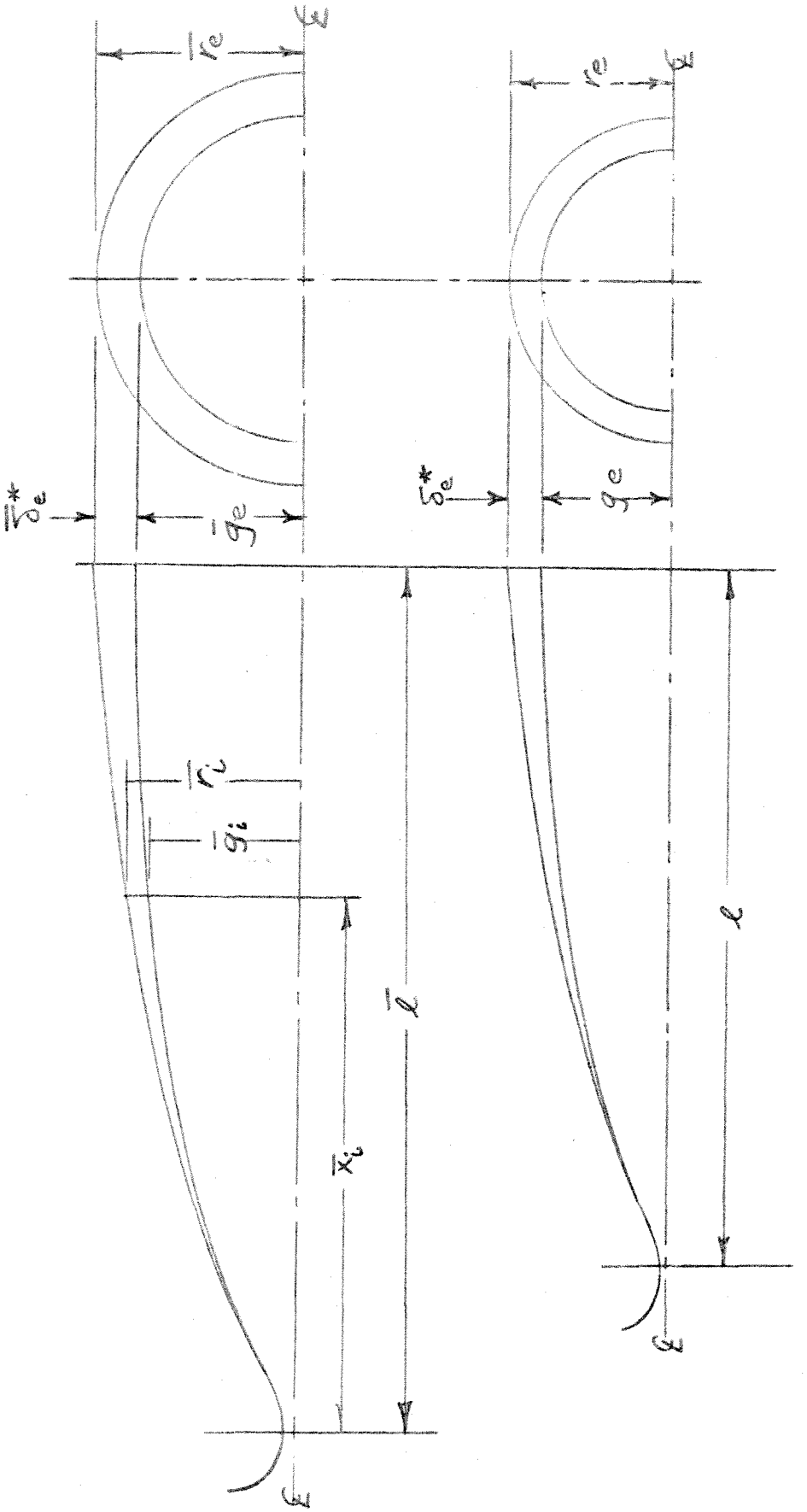

TYPE III MODIFICATION TO POTENTIAL SHAPE

FIG 18

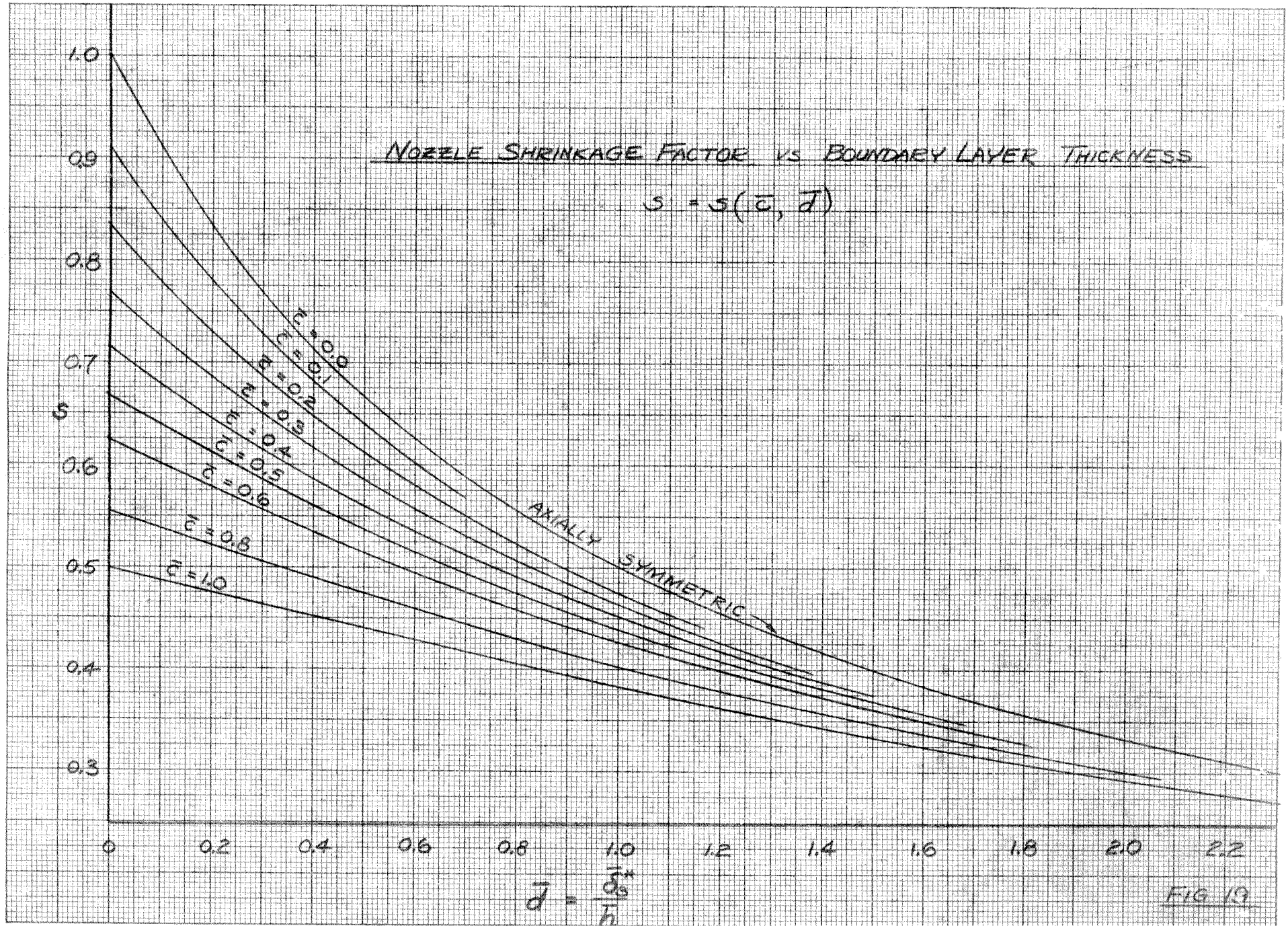
NOZZLE SHRINKAGE FACTOR VS BOUNDARY LAYER THICKNESS
$S = S(\bar{\varepsilon}, \bar{d})$
S
1.0
0.9
0.8
0.7
0.6
0.5
0.4
0.3
$\bar{\varepsilon} = 0.0$
$\bar{\varepsilon} = 0.1$
$\bar{\varepsilon} = 0.2$
$\bar{\varepsilon} = 0.3$
$\bar{\varepsilon} = 0.4$
$\bar{\varepsilon} = 0.5$
$\bar{\varepsilon} = 0.6$
$\bar{\varepsilon} = 0.8$
$\bar{\varepsilon} = 1.0$
AXIALLY SYMMETRIC
0
0.2
0.4
0.6
0.8
1.0
1.2
1.4
1.6
1.8
2.0
2.2
$\bar{d} = \frac{\bar{\delta}_3^*}{h}$

FIG 19

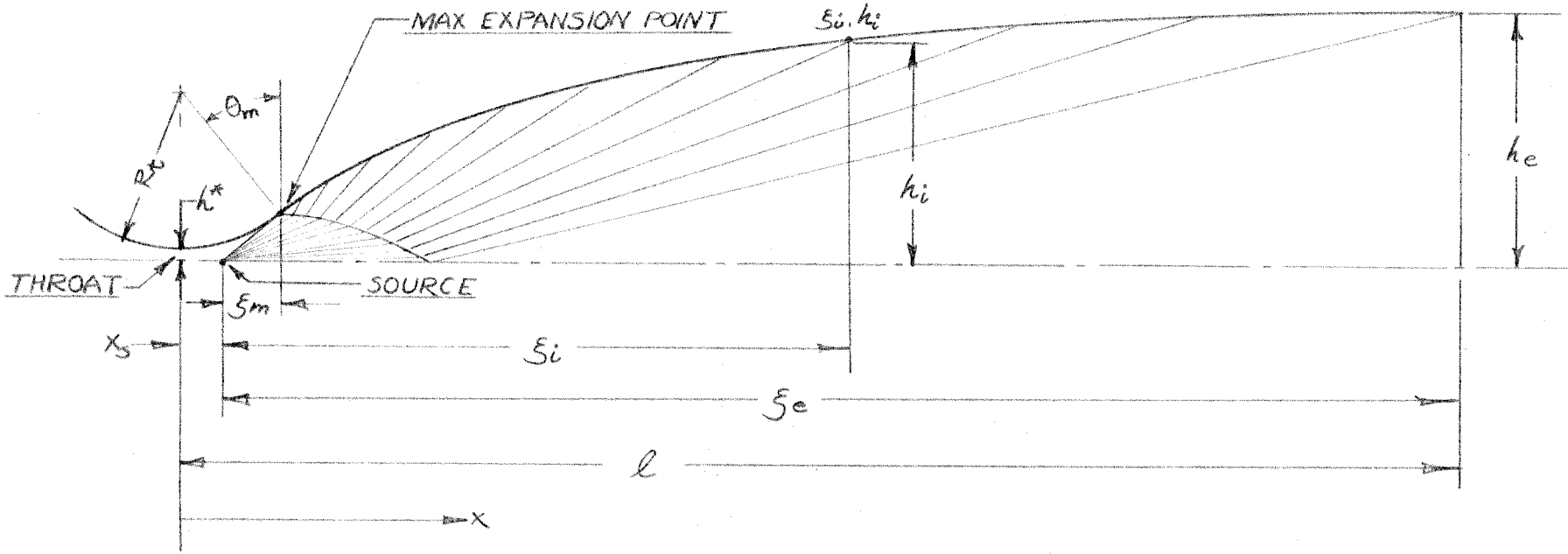

POTENTIAL NOZZLE CONFIGURATION

FIG 20

PRINCIPAL NOZZLE DIMENSIONS FOR $M = 9.88$

ψ	M	$\bar{x}_i$	$\bar{h}_i$	$\bar{\delta}^*_{2i}$	$\bar{\delta}^*_{3i}$	δ^*_{2i}	δ^*_{3i}	h_i	Δh_i	y_i	x_i
72°	4.51	1.10	0.316	0.006	0.009	0.003	0.004	0.154	0.005	0.159	0.537
80°	5.35	2.48	0.963	0.022	0.038	0.010	0.019	0.470	0.020	0.490	1.21
86°	6.15	5.75	2.055	0.072	0.130	0.035	0.063	1.003	0.066	1.069	2.806
90°	6.82	11.00	3.341	0.172	0.323	0.084	0.158	1.630	0.172	1.802	5.37
94°	7.62	22.49	5.313	0.420	0.863	0.205	0.421	2.592	0.475	3.067	10.97
96°	8.09	32.99	6.589	0.718	1.46	0.350	0.712	3.217	0.828	4.045	16.10
98°	8.62	49.34	7.995	1.250	2.54	0.610	1.24	3.900	1.49	5.390	24.08
100°	9.21	75.37	9.319	2.200	4.53	1.074	2.21	4.547	2.78	7.309	36.78
102°	9.88	117.96	10.000	3.870	8.13	1.888	3.97	4.88	5.12	10.000	57.60

$\theta_m = 30°$ $\quad \bar{R}_t = 2.21"$ $\quad \bar{h}^* = 0.01974$

$S = 0.488$ $\quad R_t = 1.08"$ $\quad h^* = 0.00963$

FIG 21

FINAL TWO DIMENSIONAL NOZZLE SHAPE

FOR M = 9.68

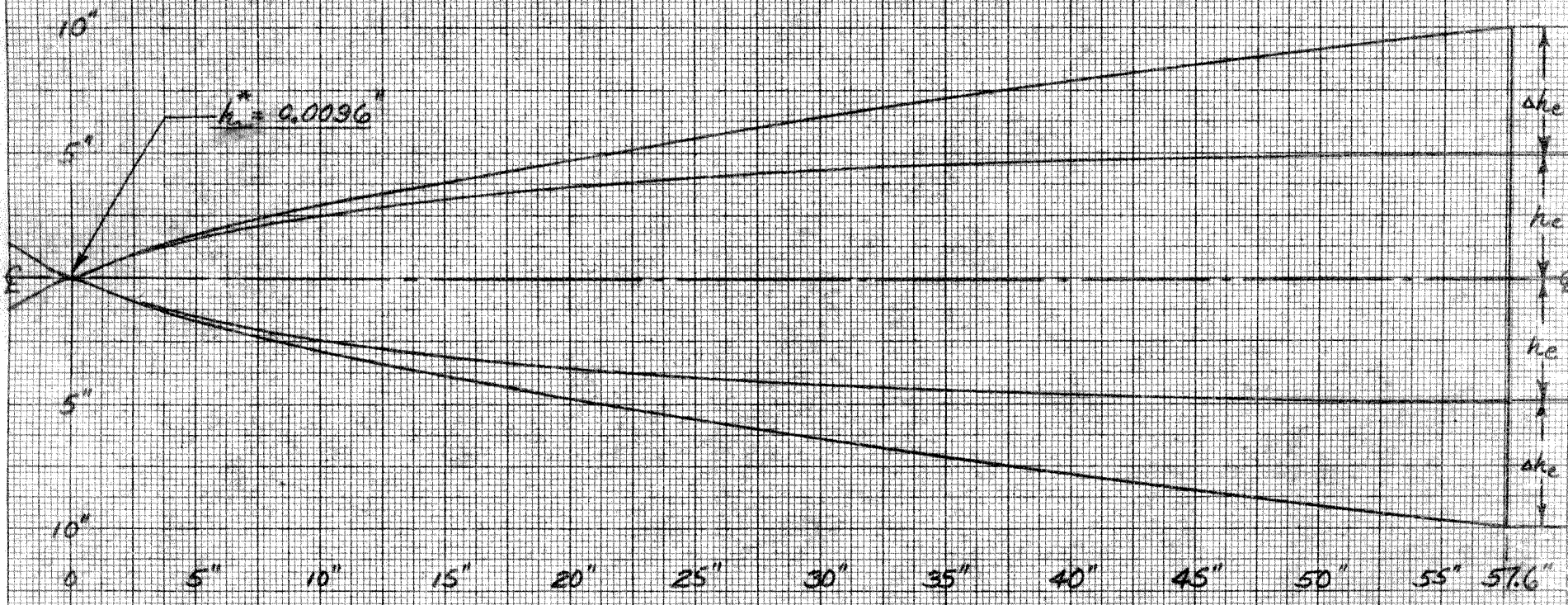

FIG 22